The staphylococcal type VII secretion system effector EsxC impacts daptomycin sensitivity through controlling bacterial cell envelope integrity

Victoria Smith[1], Giridhar Chandrasekharan[1], Robeena Farzand[1], Kate E. Watkins[1], Ramon Garcia Marset[1$], Jeannifer Yap[2], Sebastien Perrier[3], Arnaud Kengmo Tchoupa[1+], and Meera Unnikrishnan[1*].

1. Division of Biomedical Sciences, Warwick Medical School, University of Warwick, Coventry, CV4 7AL, UK.
2. Department of Chemistry, University of Warwick, Coventry, CV4 7AL, UK
3. Department of Chemistry and Warwick Medical School, University of Warwick, Coventry, CV4 7AL, UK.

$ current address: Centre for Urological Biology, Division of Medicine, University College London, WC1E 6BT London, UK.

+ current address: Cluster of Excellence EXC 2124 Controlling Microbes to Fight Infections, University of Tübingen, 72076 Tübingen, Germany

*Corresponding author m.unnikrishnan@warwick.ac.uk

Key words: Type VII secretion system, membrane integrity, membrane fluidity, daptomycin,

Abstract

The human pathogen *Staphylococcus aureus* encodes a specialised type VII secretion system (T7SS), which plays an important role in bacterial virulence during infection. However, the functions the T7SS during infection and in bacterial physiology remain unclear. Here we demonstrate that *S. aureus* strains lacking the the T7SS effector EsxC (Δ*esxC*) was highly sensitive to the important last resort drug, daptomycin, as well as other membrane-targeting antibiotics, including gramicidin and bithionol. To understand how EsxC mediates increased antibiotic sensitivity, we investigated its functions in the staphylococcal cell envelope. Scanning electron microscopy analysis of an *esxC* mutant revealed a distinct cell surface morphology. Interestingly, Δ*esxC* displayed a decrease in membrane fluidity, altered membrane protein profiles and altered cell wall synthesis. The *esxC* mutant demonstrated enhanced daptomycin binding which correlated with the increased negative charge of mutant membranes. Calcium ions, which can bind membranes affecting charge, impacted growth of Δ*esxC* and sensitivity to daptomycin, suggesting that EsxC may modulate calcium binding to membranes. Furthermore, the *esxC* mutant displayed a heightened susceptibility to daptomycin during intracellular infection, and in a murine skin infection model. Thus, our data show that the T7SS effector EsxC impacts sensitivity of *S. aureus* to membrane-acting drugs such as daptomycin through modulation of cell membrane integrity, indicating its potential as a drug target.

Author Summary T7SS has a range of functions in bacteria including specific roles in bacterial physiology including DNA uptake, membrane integrity and bacterial development. In *S. aureus* T7SS has been shown to be critical for bacterial virulence, intra-species competition and in host cell interactions, although their functions in bacterial physiology are not clear. Here we report a role of the staphylococcal T7SS effector EsxC in the modulation of the cell membrane and surface integrity, which impacts the activity of membrane targeting drugs like daptomycin. Our data indicate that targeting this system could potentially enhance activity of existing therapeutic agents.

53

54

55 **Introduction**

56 *S. aureus* is a highly versatile pathogen and a commensal bacterium which causes infections in
57 both humans and animals. Staphylococcal infections can be nosocomial or community-acquired,
58 and can range from mild skin abscesses to severe life-threatening infections including septic shock
59 and bacteraemia (1). *S. aureus* infections place a huge cost burden on healthcare sectors across
60 the world, especially due to the occurrence of antibiotic-resistant strains, such as methicillin-
61 resistant *S. aureus* (MRSA) and strains with varying levels of vancomycin resistance (2, 3).

62

63 *S. aureus* possesses an array of surface and secreted factors that help the bacterium colonise the
64 host and establish an infection (4). One such virulence-associated factor is the type VII secretion
65 system (T7SS), which is widely found in Gram positive bacteria (5). The T7SSb in *S. aureus* and
66 other firmicutes is distinct from the systems in mycobacteria (T7SSa) although both are
67 characterised by small substrates containing the WXG motif, such as EsxA and EsxB (6, 7). The
68 T7SS in *S. aureus* is modular in nature, with heterogenous expression between strains (8, 9).
69 Typically, in commonly studied *S. aureus* strains including USA300, Newman and RN6390, the
70 T7SS locus comprises of integral membrane proteins (EsaA, EssA, EssB and EssC), cytosolic
71 proteins (EsaB and EsaG), several secreted substrates (EsxA, EsxB, EsxC, EsxD and EsaD) and
72 chaperones (EsaE) (7, 10). EssC is the central transporter which is responsible for export of
73 substrates and co-dependent export of secreted substrates has been reported (6, 11). While
74 specific interactions between the different T7SS components have been described, the overall
75 structure of the secretion apparatus is poorly defined for the *S. aureus* T7SS (10, 11). Assembly
76 of a functional system is dependent on the membrane microdomain protein, flotillin A (FloA)(12).

77

78 Recent studies have reported a role for T7SS in modulation of intraspecies competition. A T7SS
79 substrate EsaD with nuclease activity mediates killing of *S. aureus* strains that lack the anti-toxin
80 EsaG (13). An LXG-domain containing protein, TspA, encoded distally to the T7SS cluster shows
81 T7SS-dependent toxic activity, which can be neutralized by an antitoxin TsaI (14). Some
82 substrates modulate host interactions during infection; EsxA modulates host cell death and EsaE
83 elicits cytokine production during infection (15, 16). However, effectors of this system are yet to
84 be defined in many *S. aureus* strains and their specific functions remain elusive.
85
86 T7SS in other bacterial species has been described to support bacterial functions like DNA
87 transfer, membrane integrity and spore development, although for *S. aureus*, it is not clear if T7SS
88 is important in staphylococcal physiology (17-19). Our recent study on the T7SS substrate EsxC
89 showed that a mutant lacking this protein was more sensitive to unsaturated host-derived fatty
90 acids (20). T7SS defects compromised membrane integrity and induced oxidative stress in
91 presence of antimicrobial fatty acids, indicating a role for these proteins in membrane
92 homeostasis. Here we report that the absence of EsxC causes an increased sensitivity to
93 membrane targeting drugs like daptomycin, both during infection *in vitro* and *in vivo*. We
94 demonstrate distinct effects on cell surface morphology, membrane fluidity and charge, indicating
95 a role for T7SS in controlling membrane integrity potentially through modulating calcium binding.
96 Our data suggest that targeting the T7SS could augment activities of membrane-acting drugs like
97 daptomycin.
98
99 **Results**
100 **A mutant lacking T7SS effector EsxC is more sensitive to membrane-acting drugs**
101 The cyclic lipopeptide antibiotic, daptomycin, is a key drug used to treat resilient *S. aureus*
102 infections. Daptomycin binds to the cell membrane in a calcium-dependent manner (21). As our
103 previous studies indicated a potential impact of T7SS, in particular the effector EsxC, on

104 membrane homeostasis (20), we investigated whether the *S. aureus* USA300 JE2 mutants lacking
105 the T7SS substrate EsxC (Δ*esxC)* respond differently to membrane-acting drugs like daptomycin.
106 Growth of Δ*esxC* was compared to the WT USA300 JE2 strain in the presence or absence of
107 daptomycin. When cultured in presence of 5 μg/ml daptomycin, growth of the WT USA300 JE2
108 strain was delayed, but growth of USA300 JE2 Δ*esxC* was significantly impaired compared to the
109 WT (Fig. 1 A). No differences in growth rates were seen between the strains in tryptic soy broth
110 (TSB) without antibiotic. Further, a 10-fold decrease in colony forming unit counts for the mutant
111 was also observed in the presence of daptomycin (Fig. 1 B). Complementing Δ*esxC* with pOS1-
112 *esxC* restored WT phenotype (Fig. 1 C, D), although daptomycin did not inhibit the pOS1 empty
113 plasmid-bearing Δ*esxC* to the same extent as Δ*esxC* without plasmid. This could be attributed to
114 differences in growth profiles of pOS1 containing WT and mutant strains, possibly due to the
115 effects of chloramphenicol exposure prior to performing growth assays. Next, a daptomycin killing
116 assay was employed where logarithmic phase bacteria were treated for 2 h with daptomycin.
117 Δ*esxC* was more sensitive to daptomycin in comparison to the WT in this killing assay, with the
118 Δ*esxC* pOS1-*esxC* strain reversing daptomycin sensitivity (Fig. 1 E, F). When we stained bacteria
119 with propidium iodide (PI), a fluorescent intercalating agent which cannot pass through the
120 membranes of viable cells, cytosols of daptomycin-treated Δ*esxC* showed a higher intensity of PI
121 compared to the WT, as quantified by fluorescence microscopy (Fig. 2 A, B). Staining with the
122 lipid staining dye FM1-43 was of similar intensity for WT and Δ*esxC*, although it appeared less
123 ordered in the daptomycin-treated Δ*esxC* sample (Fig. 2 A, B). Thus, Δ*esxC* demonstrated
124 increased membrane permeability in the presence of daptomycin.
125
126 To investigate whether other T7SS effectors had similar effects, we studied strains lacking
127 substrates EsxA and EsxB. We used mutants in USA300 LAC and Newman backgrounds, as
128 USA300 JE2 mutants in these genes were not available. A defect in growth was seen in USA300
129 LAC Δ*esxA* mutant compared to the USA300 LAC WT strain, while Δ*esxB* did not appear to have

130 a growth defect (Fig. S1 A, B). The Newman strain was more sensitive than USA300 JE2 to
131 daptomycin, with growth being delayed until ~14 h. Again a growth defect was observed for the
132 Δ*esxA* mutant, but not the Δ*esxB* mutant in presence of daptomycin (Fig. S1 C, D). Furthermore,
133 a USA300 JE2 mutant lacking another T7SS substrate, EsxD did not display any growth defects
134 in the presence of daptomycin (Fig. S1 E,F). We also studied a strain lacking and the central
135 transporter EssC (*ΔessC*) responsible for transport of T7SS effectors. As expected, the deletion
136 of *essC* significantly impaired the growth phenotype compared to the WT (Fig S1 G,H). We further
137 studied the effect of EsxC on daptomycin sensitivity in other strain backgrounds. The growth of
138 RN6390 *S. aureus* was impacted more by the addition of daptomycin, with the bacterial growth
139 initiating much later (~14 h) compared to the USA300 JE2 strain (~8 h). However, similar to the
140 JE2 mutants, RN6390 Δ*esxC* and *ΔessC* mutants were more susceptible than the WT to
141 daptomycin (Fig. S1 I, J).
142
143 To determine if the differences observed between the WT and Δ*esxC* were limited to daptomycin,
144 other membrane-targeting antimicrobials, such as gramicidin and bithionol, were tested.
145 Gramicidin is a polypeptide antimicrobial peptide that forms ion channels in the cell membrane
146 allowing diffusion of monovalent ions such as potassium (K^+) and sodium (Na^+), disrupting cell ion
147 concentrations. Bithionol is an inhibitor of soluble adenylyl cyclase and its membrane-disrupting
148 activity was associated with its ability to kill *S. aureus* persister cells (22). When treated with 2
149 µg/ml gramicidin, the WT JE2 strain did not have any growth defects, however the Δ*esxC* mutant
150 displayed slower growth (Fig. 3 A, B). A similar defect in growth was also seen in the presence of
151 biothionol, although only a slightly slower growth was seen for the mutant in the presence of 1
152 µg/ml bithionol (Fig. 3 C,D). Finally, this effect appears to be specific to membrane-acting drugs
153 as other drugs which target the cell wall (vancomycin, oxacillin) or DNA replication (ciprofloxacin,
154 mitomycin) did not differentially affect the growth of the Δ*esxC* (or Δ*essC*) as compared to the WT
155 (Fig. S2).

156

157 ***ΔesxC* displays decreased membrane fluidity and altered membrane protein profiles**

158 Changes in membrane fluidity can affect membrane function and antibiotic sensitivity. To study
159 the effect of EsxC on membrane fluidity, we assessed the membrane fluidity of the WT and Δ*esxC*
160 mutant using multiple assays. WT and Δ*esxC* were stained with a fluorescent membrane dye
161 DiI12C, which has been used detect regions of increased fluidity in bacteria (23). As reported
162 previously for *S. aureus*, we observe a few fluid regions in the WT, and an uneven staining of the
163 membrane. In contrast, a very weak staining of the membranes was observed for the Δ*esxC*
164 mutant (Fig. 4 A), which may indicate a decrease in membrane fluidity. An alternate assay using
165 pyrene decanoic acid, an excimer-forming lipid (24), was employed to measure the fluidity of WT
166 and Δ*esxC* membranes. Compared to the WT, the cytosolic membrane of the Δ*esxC* mutant
167 showed a mild but statistically significant increase in rigidity (Fig. 4 B). Finally, membrane fluidity
168 was measured using the fluorescent dye Laurdan (6-dodecanoyl-2-dimethylaminonaphthalene)
169 which is incorporated into the membrane bilayer (25). Logarithmic phase WT cells treated with
170 laurdan showed a lower average generalized polarisation value of 0.33 compared to 0.42 for
171 *ΔesxC*, which was reversed in the complemented strain Δ*esxC* pOS1*esxC*, suggesting that the
172 membrane of the *ΔesxC* mutant is more rigid in comparison to that of the WT (Fig. 4 C).
173 Overall, the data indicate that EsxC contributes to modulation of *S. aureus* membrane fluidity.

174

175 Previously, we reported that the mutants Δ*esxC* and Δ*essC* had distinct total protein profiles with
176 and without treatment with linoleic acid (20). Given the changes seen in bacterial membranes in
177 the absence of EsxC, we examined global changes in the protein content in the membrane.
178 Membrane fractions extracted from logarithmic phase (OD_{600} = 3.0) cultures of WT and Δ*esxC*
179 were analysed by nanoLC-ESI-MS/MS. 13 proteins were altered in abundance [log2 (fold change)
180 = 1.0, $P < 0.05$] in Δ*esxC* in relation to the WT (Table 1). Membrane proteins were increased in
181 abundance and EssD, a T7SS substrate and nuclease, was decreased significantly in the

182 membranes of Δ*esxC.* A secretome analysis from culture supernatants was also performed, which
183 showed a lower abundance of substrates EsxA and EssD in Δ*esxC* compared to WT (Table S1).
184 Thus, the *esxC* mutant show distinct changes to the overall membrane protein profiles and
185 secretion of certain T7SS substrates appear to be co-dependent on substrate EsxC.
186
187 **EsxC displays altered cell surface morphology and decreased rate of cell wall synthesis**
188 As EsxC appeared to be involved in membrane function, we next examined the cell surface of
189 Δ*esxC* using scanning electron microscopy. The cell surface of WT grown to early logarithmic
190 phase have the typical smooth spherical shape of *S. aureus*. However, Δ*esxC* appears deflated
191 with dents or hollows (Fig. 5 A). The WT phenotype was restored in Δ*esxC* pOS1-*esxC*
192 complemented strain (Fig. 5 B). Interestingly, this cell surface defect is not seen in all T7SS
193 mutants; strains lacking EsxD (Δ*esxD*) did not have a defective cell surface phenotype (Fig. S3).
194 *S. aureus* cell surface alterations were seen in USA300 (LAC) and Newman strains lacking EsxA
195 (*ΔesxA)*, but not in *ΔesxB* (Fig. S3). However, RN6390 strains lacking *esxC* showed very little
196 surface defects (Fig. S3). Finally the JE2 transporter mutant Δ*essC* showed defects similar to
197 Δ*esxC* (Fig S3). Differences seen in surface morphologies between WT and mutants were not
198 due to growth rate differences, as growth rates of all mutant strains in the different strain
199 backgrounds (*ΔessC*, *ΔesxC*, *ΔesxA*, Δ*esxB,* and *ΔesxD)* in TSB were similar to that of their WT
200 (Fig. S1). Our data suggest that the cell envelopes of mutants lacking specific T7SS components
201 were altered, potentially due to a defect in the cell membrane and/or cell wall structure.
202
203 To investigate if the surface structure changes were associated with a defect in cell wall structure
204 or synthesis, transmission electron microscopy was undertaken. However, there were no clear
205 differences in cell wall thickness between strains (Fig. S4). To study whether peptidoglycan
206 synthesis and accumulation were affected in the T7SS mutants, HADA, a fluorescent D-amino
207 acid was used (26). The dye was either added to a fresh subculture and grown until the bacteria

208 reached logarithmic phase or added for 10 min once the culture reached an OD_{600} of 1. No
209 differences were observed in the cells which had been grown with TSB supplemented with HADA
210 (Fig. 6 A, B), however addition of HADA during exponential phase growth revealed a faster
211 accumulation of HADA in the WT compared to *ΔesxC* (Fig. 6 A, C). This suggests that T7SS
212 mutants displayed a decreased rate of new peptidoglycan synthesis.
213
214 **Δ*esxC* displays an increased negative cell surface charge and increased binding of**
215 **daptomycin**
216 As we observed cell surface defects and changes to peptidoglycan synthesis, we next tested if
217 the deletion of *esxC* could alter other cell surface properties like surface charge. A cytochrome
218 binding assay was employed to measure surface charge; the binding of cytochrome C, a highly
219 positively charged protein, is directly proportional to the net negative surface charge of *S. aureus*
220 cells (27). A significantly higher level of binding of cytochrome C to the cell surface of Δ*esxC* was
221 observed compared to the USA300 JE2 WT strain (Fig. 7 A). Similarly, Δ*esxA* also showed
222 increased levels of binding of cytochrome C (Fig. S5). This suggests that the cell surfaces of
223 Δ*esxC* and Δ*esxA* are more negatively charged. Much lower levels of cytochrome C bound to
224 USA300 LAC WT and Δ*esxB* suggesting these cell surfaces are less negative (Fig. S5). CFU
225 counts from samples after cytochrome C addition showed no differences in cell numbers and
226 therefore it is unlikely that bacterial cell numbers influenced cytochrome C binding (Fig. 7 B, Fig
227 S5). These data indicate that the T7SS effectors EsxC impacts the surface charge of *S. aureus*.
228
229 *S. aureus* has been reported to resist daptomycin through possessing a more positive surface
230 charge, causing electrostatic repulsion of the positively charged daptomycin calcium complex, and
231 thus preventing binding (28, 29). Based on the increased negative surface charge observed for
232 the T7SS mutants in the cytochrome C assay, we hypothesised that daptomycin could bind more
233 easily in the absence of a functional T7SS. To test this, daptomycin was tagged with BODIPY and

234 used to quantify binding via fluorometry (Fig. 7C) and to visualise bound daptomycin by
235 fluorescence microscopy (Fig 7D). In the presence of daptomycin, a higher level of daptomycin
236 was observed to bind around the septum for the WT as reported previously (30). *ΔesxC* showed
237 significantly higher fluorescence in comparison to the WT. Thus, our data suggest that reduced
238 electrostatic repulsion of daptomycin may contribute to the increased daptomycin binding in
239 *ΔesxC*.
240
241 **Calcium affects the growth of *ΔesxC* and sensitivity to daptomycin**
242 Calcium is an important component in membranes, and affects both structure and charge of
243 bacterial membranes (31). Calcium is also required for the activity of daptomycin and can enhance
244 killing by gramicidin (32, 33). We hypothesied that EsxC may control membrane integrity through
245 modulating the membrane binding of calcium. To test this, EsxC mutants were cultured in minimal
246 medium with or without calcium chloride (50 mM). While both WT and mutant strains showed slow
247 growth in minimal medium in the absence of calcium, in the presence of 50 mM calcium chloride
248 the mutant grew much slower than the WT and the *esxC*-complemented strains (Fig 8 A,B,C).
249 We then examined if the daptomycin toxicity was dependent on the concentration of calcium
250 available. WT, *ΔesxC*, and the complemented strains were cultured in the presence of 5 μg/ml
251 daptomycin and increasing calcium chloride concentrations (0 to 20 mM). In the absence of
252 calcium, the daptomycin did not have any effect as expected. A dose-dependent decrease in
253 growth of the WT strain was observed with increasing concentrations of calcium chloride with the
254 WT showing slower growth at 10 mM and 20 mM $CaCl_2$ compared to 1 mM (Figure 8 D, Fig S6).
255 The mutant was more sensitive to daptomycin at all calcium concentrations compared to the WT
256 and complemented strains, with increased growth inhibition at higher $CaCl_2$ concentrations .
257 Hence calcium binding to membranes and/or downstream signalling may be impacted in the
258 *ΔesxC*, affecting its ability to grow in presence of calcium and its sensitivity to membrane targeting
259 drugs like daptomycin.

260

261 **Decreased survival of EsxC mutants during intracellular infection with daptomycin**

262 *S. aureus* is a facultative intracellular pathogen, and daptomycin is considered to kill intracellular
263 bacteria effectively. Hence, to determine if deletion of *esxC* from *S. aureus* would enhance
264 intracellular killing activity, A549 human lung epithelial cells (15) were infected with *S. aureus* and
265 treated with a high concentration of daptomycin (20 µg/ml). While there were no differences in the
266 bacterial numbers between the WT and T7SS mutant in internalised bacteria (1 h after infection),
267 a significant decrease was observed in the numbers of Δ*esxC* surviving within cells treated with
268 daptomycin in comparison to WT after 4 h and 24 h after infection (Fig. 9 A). Notably, there was a
269 significant number of WT *S. aureus* bacteria surviving intracellularly after treatment with
270 daptomycin. Confocal microscopy imaging of infected cells also showed similar number of
271 bacterial cells invading or internalized by mammalian cells but more *S. aureus* WT remaining 24
272 h after infection compared to *ΔesxC* in presence of daptomycin (Fig. 9 B, C). The differences seen
273 in the infection assay were not due to the ability of the mutants to grow differently in DMEM-10,
274 as strains had similar growth rates (Fig. S7A), with a growth defect in presence of daptomycin as
275 expected (Fig. S7B). Therefore, our data suggest that daptomycin is more effective in killing
276 intracellular *S. aureus* in the absence of T7SS.

277

278 ***S. aureus* lacking EsxC is sensitive to daptomycin in a skin infection model**

279 As T7SS proteins have been reported to be important in various murine infection models (6, 8,
280 34), we next investigated effects of daptomycin on *S. aureus* infection and the impact of EsxC on
281 daptomycin killing *in vivo* employing a localised murine skin abscess model. 7-8-week-old BALB/c
282 mice were infected with *S. aureus* WT and *ΔesxC* intradermally, followed by treatment
283 (intravenous) 2 h post infection (h.p.i) and every 24 h thereafter with 10 mg/kg daptomycin.
284 Bacterial counts were obtained from skin tissue 24 or 72 h.p.i. Weight and skin lesion diameters
285 were recorded every day. In the non-treated groups, bacterial counts from the site of infection

286 (lesions) showed no significant difference between WT and *ΔesxC* infected mice after 24 or 72 h
287 of infection. A significant decrease was seen in the numbers of *ΔesxC* present in the skin of
288 daptomycin-treated mice compared to the untreated group 24 and 72 h.p.i, while this was not the
289 case for the WT-infected group. (Fig. 8A and B). No significant differences were observed between
290 the areas of lesions measured for WT or *ΔesxC* after 24 h or 72 h infections and in daptomycin-
291 treated mice (Fig S8). Although the dose of daptomycin used in the time-frame of treatment was
292 not sufficient to treat WT *S. aureus* infection, this data suggests that the strain lacking EsxC was
293 more susceptible to daptomycin *in vivo* compared to the WT.
294
295 **Discussion**
296 The *S. aureus* T7SS has been strongly associated with staphylococcal virulence and the ability of
297 this pathogen to persist during infection (7). Its importance for bacterial competition between *S.*
298 *aureus* strains has been recently highlighted (13). However, the role of this system in
299 staphylococcal physiology has been poorly defined. Here we report that EsxC, a T7SS effector is
300 critical in maintaining cell membrane homeostasis through modulating membrane properties
301 including fluidity, accompanied by changes in membrane protein localisation, changes to the rate
302 of cell wall synthesis and surface charge. Our data indicate that EsxC may mediate these
303 membrane effects through modulating calcium binding to the membrane. Consequently, EsxC
304 impacts activity of membrane acting drugs including daptomycin, a key drug used to treat resilient
305 staphylococcal infections. Our data demonstrate that EsxC can modulate the activity of
306 daptomycin both intracellularly as well as during infection *in vivo*.
307
308 Several studies in mycobacterial species have linked the T7SS to cell surface integrity in different
309 ways (19, 35-38). The ESX-1 system has been previously reported to impact cell membrane
310 permeability in *M. tuberculosis*, although this effect appeared to be strain specific (35). However,
311 ESX-5 which is considered essential for *in vitro* growth, has been linked to mycobacterial capsular,

312 cell wall and outer membrane permeability (19, 36, 39). As ESX-5 was no longer essential in *M.*
313 *marinum* when the membrane was permeabilised, it was proposed that ESX-5 mediates transport
314 of cell envelope proteins to the outer membrane required for uptake of essential nutrients. While
315 these substrates have not been identified, a substrate PPE-10 was associated with capsular
316 integrity (19, 36). In *S. aureus,* we previously reported that the effectors, EsxC, and the ATPase,
317 EssC, were associated with maintenance of membrane integrity in response to antimicrobial host
318 fatty acids (20). T7SS proteins have been previously linked to membrane fluidity. Higher levels of
319 T7SS transcription were associated with a decrease in membrane fluidity, caused by the fatty acid
320 kinase complex, which incorporates host fatty acids into the membrane, inducing a change in
321 membrane dynamics (24).
322
323 To explain the membrane defects associated with EsxC we considered multiple possibilities; 1.
324 EsxC affects other membrane-associated proteins, impacting the lipid packing and fluidity of the
325 membrane; EsxC may be a chaperone for membrane proteins and play a role in targeting them
326 to the membrane. A recent bacterial two-hybrid library screening we performed was not successful
327 in identifying any direct bacterial interactors, however it is possible that such interactions are
328 transient. 2. EsxC may impact the state of the membrane by binding other molecules like metal
329 ions required for maintaining stability of the membrane (40). 3. T7SS substrates are secreted in a
330 co-dependent manner, so EsxC-mediated effects may be attributed to another T7SS substrate
331 like EsxA. Our data indicate that the T7SS substrates may be involved in modulating metal binding
332 to the membrane.
333
334 Calcium and other metal ions like magnesium are known to impact structure and function of
335 bacterial membranes (31, 41, 42). Calcium maintains bacterial outer membrane structure through
336 binding to bacterial lipopolysaccharide, and also influences bacterial membrane fluidity (43, 44).
337 Calcium can also have antibacterial effects; higher concentrations of calcium can disrupt

338 membrane integrity (42, 45, 46). Calcium affects the growth of *S. aureus* lacking EsxC indicating
339 that the protein may modulate calcium binding to the membrane. EsxC may directly or with other
340 T7SS effectors or membrane proteins, bind to calcium, and/ or be involved in transporting or
341 modulating calcium binding to the cell envelope. The molecular mechanisms underlying calcium
342 interactions of EsxC/ other T7SS substrates need further investigation.
343
344 It is also interesting that not all T7SS substrates have a cell surface associated defect which
345 indicates substrate specificity. EsxD and EsxB did not appear to be associated with surface
346 morphology defects by SEM as observed for EsxC and EsxA. Surface charges corelated well with
347 daptomycin sensitivity indicating that these substrates did not play a role in the membrane
348 homeostasis. Surface charge measurements of WT and mutants using a cytochrome C binding
349 assay revealed that Δ*esxC* and Δ*esxA* had an increased negative surface charge, whereas *ΔesxB*
350 did not display any differences in charge to the WT. The *esxC* and *essC* RN6390 strains however
351 did not show similar differences by SEM, which may be due to differences in global regulatory
352 circuits that may control cell wall synthesis (Agr, Sar) (47-49).
353
354 While *esxA* is conserved across all *S. aureus* strains, *esxC* is only found in the *essC1* locus (8, 9).
355 It is however likely that all *S. aureus* strains encode a protein orthologous to EsxC as proteins in
356 module 2, with variants essC2-4, have not yet been characterised and could function like EsxC.
357 Additionally, common phenotypes were seen for strains which lacked EsxC or EsxA. Previous
358 reports have suggested that EsxC and EsxA interact (11). Also, our previous study showed no
359 differences in esxA levels in Δ*esxC* total cell lysates, but we find decreased EsxA in the Δ*esxC*
360 secretome indicating co-dependent secretion of EsxA and EsxC (20). Therefore, interactions
361 between EsxC and EsxA may be important in modulating membrane integrity.
362

363 Daptomycin is thought to bind to the cell membrane before forming a complex with cell wall
364 biosynthesis machinery, preventing cell wall synthesis, before dispersing throughout the bacterial
365 membrane causing depolarisation (50). Daptomycin, although not a cationic antimicrobial peptide,
366 forms a highly positively charged complex with calcium to become active (50). Significantly more
367 daptomycin was bound to *ΔesxC* than the WT, which supports the hypothesis that the decrease
368 in surface charge measured in *ΔesxC* allows easier binding of daptomycin to the cell membrane.
369 In agreement with this, T7SS substrates may influence the free calcium available for activating
370 daptomycin. Daptomycin has also been reported to affect bacterial membrane fluidity through
371 perturbing membrane microdomains (51). Clinical daptomycin resistant isolates have generally
372 been associated with increased fluidity which is not associated with changes in fatty acid content
373 (52, 53). As we show that EsxC can impact membrane fluidity, it could further contribute to
374 daptomycin resistance by altering membrane fluidity and charge. Daptomycin resistance in *S.*
375 *aureus* has been mainly associated with mutations in genes encoding for multipeptide resistance
376 factor (MprF), a lipid biosynthetic enzyme, and the vancomycin-resistance associated
377 sensor/regulator (VraSR), two component systems (54-56). Genome sequencing did not reveal
378 any changes in the *ΔesxC* genome, and a proteomic analysis of mutant whole lysates did not
379 show any modulation of proteins implicated in daptomycin resistance (20).
380
381 In contrast to daptomycin, bithionol and gramicidin are uncharged (22, 57), therefore surface
382 charge and thus decreased electrostatic repulsion of the antibiotics is not the only factor involved
383 in increased sensitivity of the EsxC mutant, although calcium is known to increase gramicidin
384 activity (32). As all three antimicrobials have different mechanisms of action once bound to the
385 membrane, before causing membrane depolarization, the subsequent steps after membrane
386 binding appear to be important for efficacy. Therefore, daptomycin treatment which impacts both
387 the cell membrane, and the cell wall causes a larger effect in the the EsxC mutant.
388

389 While daptomycin kills the *esxC* mutant *in vivo*, at the dose and with the strains of *S. aureus* used,
390 there was no impact of the EsxC in bacterial survival during acute skin infection. T7SS proteins
391 have been previously reported to be important for bacterial virulence using invasive kidney
392 abscess, nasal colonisation and skin infection models, although studies have used different *S.*
393 *aureus* strains (6, 8, 34). The lack of decrease in the lesion size of the T7SS mutant-infected mice
394 treated with daptomycin, unlike the trend towards decreased lesion size observed for the WT (Fig
395 S7), could indicate that the increased killing of bacteria may cause an altered local immune
396 response. A recent study reported that in a *S. aureus* strain WU1, the T7SS was important only
397 for invasive infection and not localized nasal colonization (58).
398
399 Currently, levels of resistance to daptomycin are low, however, with increasing resistance in other
400 last line antibiotics, such as vancomycin, the use of daptomycin going forward will increase (59).
401 The increased use of daptomycin will likely lead to the occurrence of more resistant isolates,
402 therefore research into new antibiotics, and targeting new proteins that can enhance existing
403 treatments could be a powerful approach. Our data indicate that inhibitors of T7SS proteins or of
404 T7SS secretion could have excellent potential in combination drug therapies.
405
406 **Materials and Methods**
407 **Bacterial strains***: S. aureus* strains used in this study are included in Table 2. Strains were
408 cultured aerobically in tryptic soy broth (TSB) (Sigma-Aldrich) at 37°C with aeration at 180 rpm
409 overnight. Overnight cultures were subcultured into fresh TSB and grown to a density of optical
410 density (OD_{600}) of 1, unless stated otherwise. For complemented strains TSB was supplemented
411 with 10 µg/ml chloramphenicol.
412 **Growth curves**: Overnight bacterial cultures were diluted to an OD_{600} of 0.1 in TSB or TSB
413 supplemented with antimicrobials where specified. Bacteria were grown in a 96-well plate with

414 shaking and the OD_{600} was measured every 15 min with a FLUOstar OMEGA plate reader (BMG
415 Labtech, UK). At appropriate time points 100 µl of the samples were taken for CFU determination.
416 For growth curves in defined medium, overnight cultures were subcultured into minimal defined
417 media, prepared as described by Machado and colleagues (60), at an initial OD_{600} of 0.15, and
418 supplemented with varying concentrations of $CaCl_2$ where stated. Bacterial growth was monitored
419 manually by measuring OD_{600} at different time points using a spectrophotometer (Biochrom), due
420 to issue with increased bacterial clumping in this medium on microtitre plates. 100 µl of the
421 samples were also taken for CFU determination at different time points.
422 **Daptomycin killing assays**: Bacterial cultures were grown overnight in TSB, diluted to an OD_{600}
423 of 0.15 and grown to log phase. Bacterial cultures were then treated with 10 µg/ml of daptomycin
424 (Acros Organics) in the presence of 1 mM $CaCl_2$ (Fisher Scientific) and incubated at 37ºC for a
425 further 2 h. Aliquots were removed at indicated timepoints, serially diluted in PBS and plated on
426 tryptic soy agar (TSA) for CFU determination.
427 **Scanning Electron Microscopy**: Overnight bacterial cultures were diluted to an OD_{600} of 0.15
428 and grown to an OD_{600} of 1 in TSB. The pellet was washed with PBS twice before dropping onto
429 poly-lysine coated 12 mm circular coverslips. Samples were fixed with 2.5% glutaraldehyde in
430 PBS for 1 h at 4°C. The bacterial cells were dehydrated by washing with a series of ethanol
431 solutions (20%, 50%, 70%, 90% and 100%) and dried with hexamethyldisilazane. The samples
432 were sputter coated with carbon and then observed using a Gemini SEM 500 (Zeiss).
433 **Laurdan staining:** Membrane fluidity was measured using the fluorescent dye Laurdan (Sigma)
434 and was based on protocols described by Wenzel and colleagues (61). Logarithmic phase *S.*
435 *aureus* was grown, and 1 ml aliquots were washed in PBS. The samples were incubated with a
436 final concentration of 100 µM Laurdan for 5 minutes at 37°C in the dark. Samples were washed
437 four times in pre-warmed PBS and 200 µl was transferred to a pre-warmed black walled 96 well
438 plate in triplicate. Membrane fluidity was determined by using an excitation wavelength of 350 nm
439 and measuring fluorescence at 460 nm and 500 nm emission wavelengths on a BioTek Cytation

440 5 Cell Imaging Multimode Reader (Agilent). The generalised polarisation (GP) value was
441 calculated using the following calculation, GP = $(I_{460}-I_{500}) / (I_{460}+I_{500})$.
442 **Pyrene decanoic acid staining**: O/N bacterial cultures were diluted to an OD_{600} of 0.15 in TSB
443 and were grown to an OD_{600} of 1.0. Bacteria were washed with PBS prior to treatment for 30 min
444 at 37ºC with 37.5 µg/mL lysostaphin in PBS containing 20% sucrose. The spheroblasts were then
445 centrifuged at 8000 × g for 10 min, and the pellet resuspended in the labelling solution (PBS, 20%
446 sucrose, 0.01% F-127, 5 µM pyrene decanoic acid). The incubation in the dark was done for 1h
447 at 25ºC under gentle rotation. PBS supplemented with 20% sucrose was used to wash the stained
448 spheroblasts that were afterwards transferred to 96-well plates for fluorescence 450 nm
449 measurements as previously described (24).
450 **DiIC12 staining:** O/N bacterial cultures were diluted to an OD_{600} of 0.15 in TSB with 1 µg/mL 1,1′-
451 didodecyl-3,3,3′,3′-tetramethylindocarbocyanine perchlorate (DiIC12) (Invitrogen). Cultures were
452 grown to an OD_{600} of 1.0, centrifuged and washed twice with fresh TSB. Samples were spotted on
453 to agarose pads and imaged using a Leica DMi8 widefield microscope (Leica Microsystems, UK).
454 Acquired images were analysed with the ImageJ processing package, Fiji.
455 **Cytochrome C binding assay**: Overnight bacterial cultures were pelleted and washed with 20
456 mM MOPS buffer, pH 7. The cells were resuspended in MOPS buffer at an OD_{600} of 1 and
457 incubated with 50 µg/ml cytochrome C at room temperature for 15 min. The cells were pelleted
458 and the remaining cytochrome C in the supernatant was measured spectrophotometrically at
459 OD_{410} using a FLUOstar OMEGA plate reader (BMG Labtech, UK).
460 **HADA incorporation assay**
461 Peptidoglycan synthesis was investigated by measuring HCC-amino-D-alanine (HADA)
462 incorporation. Overnight *S. aureus* cultures were diluted into TSB supplemented with 25 µM HADA
463 and incubated at 37ºC in the dark. When OD_{600} of 1 was reached cultures were washed three
464 times and fixed with 4% PFA. Alternatively, cultures were treated with daptomycin for 30 min.

465 before washing and fixing. Microscopy was undertaken on these samples using the DAPI filter set
466 on a Leica DMi8 widefield microscope.

467 **Daptomycin BODIPY binding assay***: S. aureus* was grown as previously described and treated
468 with 1μg/ml daptomycin-BODIPY once logarithmic phase had been reached. The samples were
469 incubated at 37ºC for 30 min in the dark, then washed with PBS three times. 200 µl were aliquoted
470 into black 96 well plates in triplicate and fluorescence was measured using a BioTek Cytation 5
471 Cell Imaging Multimode Reader (Agilent). The excitation wavelength used was 488 nm and
472 emission wavelength used was 530 nm.

473 **Invasion and survival assays**: Infection assays were carried out in 24 well tissue culture treated
474 plates (Falcon), or RS treated glass chamber slides (154526, Nunc, Lab Tek II). Overnight *S.*
475 *aureus* cultures were diluted to an OD_{600} of 0.15 and grown to an OD_{600} of 1. Cultures were
476 resuspended in DMEM media to a density of 2.5 x 10^6 CFU/ml. A549 epithelial cells were seeded
477 in 24 well plates at a density of 2.5 x 10^5 one day before being infected with *S. aureus* at a
478 multiplicity of infection (MOI) of 10. Cells were infected for 1 h at 37°C with 5 % CO_2. To kill any
479 extracellular bacteria, cells were washed with DMEM media containing 20 µg/ml lysostaphin
480 (Sigma-Aldrich) and 50 µg/ml gentamycin (Melford) and incubated for a further 30 minutes. Cells
481 were washed twice with PBS, lysed with 1 ml cold sterile water and vigorous pipetting before
482 plating for CFU determination. To investigate the course of infection after extracellular bacterial
483 killing, the cells are washed twice with PBS and refreshed with DMEM with 1 mM $CaCl_2$ only, or
484 DMEM supplemented with 1 mM $CaCl_2$ and 10 µg/ml daptomycin and incubated until the desired
485 timepoint. The above protocol to lyse the cells is then followed.

486 **Murine skin abscess model:** All animal procedures were carried out as per protocols in the
487 Project Licence PCEC27E7D. All local ethical and home office approvals were obtained for animal
488 experimentation. For the murine skin abscess model, female 7/8-week-old BALB/c mice (Charles
489 River Laboratories, UK) flanks were shaved before injection, and inoculated through an
490 intradermal route with 50 µl of bacterial suspension per flank (one injection on each flank),

491 resulting in a final bacterial count of 1-2 x 10^6 per mouse. Overnight *S. aureus* cultures were
492 subcultured, grown to OD_{600} of 1, centrifuged and washed twice with PBS, and diluted in PBS to
493 achieve a final CFU/ml of 1-2 x 10^7 for infection. 2 h after infection mice were given an intravenous
494 dose of daptomycin or PBS via tail vein injection. This was repeated once every 24 h. During the
495 experiment, mice were weighed daily, and any abscess formation was measured and recorded.
496 After 24 h or 72 h mice were euthanised by CO_2 inhalation and skin at the infection site was
497 incised. The skin samples were weighed and homogenised in PBS using a FastPrep (MP
498 Biomedicals), at 4 m/s for 60 seconds for a total of 6 cycles. Homogenates were diluted in PBS
499 and CFU/ml was determined. CFU counts were normalized to lesion weight.
500 **Statistical Analysis**: All experiments were performed at least three independent times. Statistical
501 analysis was performed using GraphPad Prism 9.0 (MacOS version 9.5.1). Pairwise statistical
502 analysis was carried out by the Mann-Whitney U test or t test? for two groups, or One way
503 ANOVAs for multiple groups, followed by post-hoc Tukey's HSD tests where necessary.
504 Significance was denoted by asterisks; * = $P < 0.05$, ** = $P < 0.01$, *** = $P < 0.001$, **** = $P <$
505 0.0001 and ns = not significant.
506

507 **Acknowledgements**

508 We would like to acknowledge funding from MIBTP (grant 2097375) to Victoria Smith and the
509 Medical Research Council grants (MR/N010140/1 and MR/X00161X/1) for funding.
510 We would like to thank Novartis Vaccines, Siena (GSK biologicals) Italy for providing the *ΔesxA*
511 and *ΔesxB* strains, and Prof Tracy Palmer for providing the RN6390 *ΔesxC* and *ΔessC* strains,
512 used in this study. We acknowledge the Midlands Regional Cryo-EM Facility, hosted at the
513 Warwick Advanced Bioimaging Research Technology Platform, for the use of the JEOL 2100Plus.
514

515 **Author contributions**

516 VS, AKT and MU conceptualised ideas, designed experiments, VS, GC, RF, KEW, RGM, JY, AKT
517 conducted experiments, MU and SP provided resources for the study, VS, AKT, GC, KEW, RGM,
518 RF and MU analysed data, AKT and MU supervised study, MU, VS, RF and AKT drafted
519 manuscript and all authors were involved in reviewing manuscript draft.

520

521 **References**

522 1. Tong SY, Davis JS, Eichenberger E, Holland TL, Fowler VG, Jr. 2015. Staphylococcus aureus
523 infections: epidemiology, pathophysiology, clinical manifestations, and management. Clin
524 Microbiol Rev 28:603-61.
525 2. Chambers HF, Deleo FR. 2009. Waves of resistance: Staphylococcus aureus in the antibiotic
526 era. Nat Rev Microbiol 7:629-41.
527 3. Lee BY, Singh A, David MZ, Bartsch SM, Slayton RB, Huang SS, Zimmer SM, Potter MA,
528 Macal CM, Lauderdale DS, Miller LG, Daum RS. 2013. The economic burden of community-
529 associated methicillin-resistant Staphylococcus aureus (CA-MRSA). Clin Microbiol Infect
530 19:528-36.
531 4. Cheung GYC, Bae JS, Otto M. 2021. Pathogenicity and virulence of Staphylococcus aureus.
532 Virulence 12:547-569.
533 5. Bottai D, Groschel MI, Brosch R. 2016. Type VII Secretion Systems in Gram-Positive
534 Bacteria. Curr Top Microbiol Immunol doi:10.1007/82_2015_5015.
535 6. Burts ML, Williams WA, DeBord K, Missiakas DM. 2005. EsxA and EsxB are secreted by an
536 ESAT-6-like system that is required for the pathogenesis of Staphylococcus aureus
537 infections. Proc Natl Acad Sci U S A 102:1169-74.
538 7. Unnikrishnan M, Constantinidou C, Palmer T, Pallen MJ. 2017. The Enigmatic Esx Proteins:
539 Looking Beyond Mycobacteria. Trends Microbiol 25:192-204.
540 8. Kneuper H, Cao ZP, Twomey KB, Zoltner M, Jager F, Cargill JS, Chalmers J, van der Kooi-Pol
541 MM, van Dijl JM, Ryan RP, Hunter WN, Palmer T. 2014. Heterogeneity in ess transcriptional
542 organization and variable contribution of the Ess/Type VII protein secretion system to
543 virulence across closely related Staphylocccus aureus strains. Mol Microbiol 93:928-43.
544 9. Warne B, Harkins CP, Harris SR, Vatsiou A, Stanley-Wall N, Parkhill J, Peacock SJ, Palmer T,
545 Holden MT. 2016. The Ess/Type VII secretion system of Staphylococcus aureus shows
546 unexpected genetic diversity. BMC Genomics 17:222.
547 10. Bowman L, Palmer T. 2021. The Type VII Secretion System of Staphylococcus. Annu Rev
548 Microbiol 75:471-494.
549 11. Anderson M, Aly KA, Chen YH, Missiakas D. 2013. Secretion of atypical protein substrates
550 by the ESAT-6 secretion system of Staphylococcus aureus. Mol Microbiol 90:734-43.
551 12. Mielich-Suss B, Wagner RM, Mietrach N, Hertlein T, Marincola G, Ohlsen K, Geibel S, Lopez
552 D. 2017. Flotillin scaffold activity contributes to type VII secretion system assembly in
553 Staphylococcus aureus. PLoS Pathog 13:e1006728.

554 13. Cao Z, Casabona MG, Kneuper H, Chalmers JD, Palmer T. 2016. The type VII secretion
555 system of Staphylococcus aureus secretes a nuclease toxin that targets competitor
556 bacteria. Nat Microbiol 2:16183.
557 14. Ulhuq FR, Gomes MC, Duggan GM, Guo M, Mendonca C, Buchanan G, Chalmers JD, Cao Z,
558 Kneuper H, Murdoch S, Thomson S, Strahl H, Trost M, Mostowy S, Palmer T. 2020. A
559 membrane-depolarizing toxin substrate of the Staphylococcus aureus type VII secretion
560 system mediates intraspecies competition. Proc Natl Acad Sci U S A 117:20836-20847.
561 15. Korea CG, Balsamo G, Pezzicoli A, Merakou C, Tavarini S, Bagnoli F, Serruto D, Unnikrishnan
562 M. 2014. Staphylococcal Esx proteins modulate apoptosis and release of intracellular
563 Staphylococcus aureus during infection in epithelial cells. Infect Immun 82:4144-53.
564 16. Anderson M, Ohr RJ, Aly KA, Nocadello S, Kim HK, Schneewind CE, Schneewind O,
565 Missiakas D. 2017. EssE Promotes Staphylococcus aureus ESS-Dependent Protein Secretion
566 To Modify Host Immune Responses during Infection. J Bacteriol 199.
567 17. Fyans JK, Bignell D, Loria R, Toth I, Palmer T. 2013. The ESX/type VII secretion system
568 modulates development, but not virulence, of the plant pathogen Streptomyces scabies.
569 Mol Plant Pathol 14:119-30.
570 18. Flint JL, Kowalski JC, Karnati PK, Derbyshire KM. 2004. The RD1 virulence locus of
571 Mycobacterium tuberculosis regulates DNA transfer in Mycobacterium smegmatis. Proc
572 Natl Acad Sci U S A 101:12598-603.
573 19. Ates LS, Ummels R, Commandeur S, van de Weerd R, Sparrius M, Weerdenburg E, Alber
574 M, Kalscheuer R, Piersma SR, Abdallah AM, Abd El Ghany M, Abdel-Haleem AM, Pain A,
575 Jimenez CR, Bitter W, Houben EN. 2015. Essential Role of the ESX-5 Secretion System in
576 Outer Membrane Permeability of Pathogenic Mycobacteria. PLoS Genet 11:e1005190.
577 20. Kengmo Tchoupa A, Watkins KE, Jones RA, Kuroki A, Alam MT, Perrier S, Chen Y,
578 Unnikrishnan M. 2020. The type VII secretion system protects Staphylococcus aureus
579 against antimicrobial host fatty acids. Sci Rep 10:14838.
580 21. Huang HW. 2020. DAPTOMYCIN, its membrane-active mechanism vs. that of other
581 antimicrobial peptides. Biochim Biophys Acta Biomembr 1862:183395.
582 22. Kim W, Zou G, Hari TPA, Wilt IK, Zhu W, Galle N, Faizi HA, Hendricks GL, Tori K, Pan W, Huang
583 X, Steele AD, Csatary EE, Dekarske MM, Rosen JL, Ribeiro NQ, Lee K, Port J, Fuchs BB,
584 Vlahovska PM, Wuest WM, Gao H, Ausubel FM, Mylonakis E. 2019. A selective membrane-
585 targeting repurposed antibiotic with activity against persistent methicillin-resistant
586 Staphylococcus aureus. Proc Natl Acad Sci U S A 116:16529-16534.
587 23. Strahl H, Burmann F, Hamoen LW. 2014. The actin homologue MreB organizes the bacterial
588 cell membrane. Nat Commun 5:3442.
589 24. Lopez MS, Tan IS, Yan D, Kang J, McCreary M, Modrusan Z, Austin CD, Xu M, Brown EJ.
590 2017. Host-derived fatty acids activate type VII secretion in Staphylococcus aureus. Proc
591 Natl Acad Sci U S A 114:11223-11228.
592 25. Scheinpflug K, Krylova O, Strahl H. 2017. Measurement of Cell Membrane Fluidity by
593 Laurdan GP: Fluorescence Spectroscopy and Microscopy. Methods Mol Biol 1520:159-174.
594 26. Kuru E, Hughes HV, Brown PJ, Hall E, Tekkam S, Cava F, de Pedro MA, Brun YV,
595 VanNieuwenhze MS. 2012. In Situ probing of newly synthesized peptidoglycan in live
596 bacteria with fluorescent D-amino acids. Angew Chem Int Ed Engl 51:12519-23.

597 27. Peschel A, Otto M, Jack RW, Kalbacher H, Jung G, Gotz F. 1999. Inactivation of the dlt
598 operon in Staphylococcus aureus confers sensitivity to defensins, protegrins, and other
599 antimicrobial peptides. J Biol Chem 274:8405-10.
600 28. Bertsche U, Yang SJ, Kuehner D, Wanner S, Mishra NN, Roth T, Nega M, Schneider A, Mayer
601 C, Grau T, Bayer AS, Weidenmaier C. 2013. Increased cell wall teichoic acid production and
602 D-alanylation are common phenotypes among daptomycin-resistant methicillin-resistant
603 Staphylococcus aureus (MRSA) clinical isolates. PLoS One 8:e67398.
604 29. Mishra NN, Bayer AS, Weidenmaier C, Grau T, Wanner S, Stefani S, Cafiso V, Bertuccio T,
605 Yeaman MR, Nast CC, Yang SJ. 2014. Phenotypic and genotypic characterization of
606 daptomycin-resistant methicillin-resistant Staphylococcus aureus strains: relative roles of
607 mprF and dlt operons. PLoS One 9:e107426.
608 30. Monteiro JM, Fernandes PB, Vaz F, Pereira AR, Tavares AC, Ferreira MT, Pereira PM, Veiga
609 H, Kuru E, VanNieuwenhze MS, Brun YV, Filipe SR, Pinho MG. 2015. Cell shape dynamics
610 during the staphylococcal cell cycle. Nat Commun 6:8055.
611 31. Smith RJ. 1995. Calcium and bacteria. Adv Microb Physiol 37:83-133.
612 32. Fang ST, Huang SH, Yang CH, Liou JW, Mani H, Chen YC. 2022. Effects of Calcium Ions on
613 the Antimicrobial Activity of Gramicidin A. Biomolecules 12.
614 33. Jung D, Rozek A, Okon M, Hancock RE. 2004. Structural transitions as determinants of the
615 action of the calcium-dependent antibiotic daptomycin. Chem Biol 11:949-57.
616 34. Wang Y, Hu M, Liu Q, Qin J, Dai Y, He L, Li T, Zheng B, Zhou F, Yu K, Fang J, Liu X, Otto M, Li
617 M. 2016. Role of the ESAT-6 secretion system in virulence of the emerging community-
618 associated Staphylococcus aureus lineage ST398. Sci Rep 6:25163.
619 35. Garces A, Atmakuri K, Chase MR, Woodworth JS, Krastins B, Rothchild AC, Ramsdell TL,
620 Lopez MF, Behar SM, Sarracino DA, Fortune SM. 2010. EspA acts as a critical mediator of
621 ESX1-dependent virulence in Mycobacterium tuberculosis by affecting bacterial cell wall
622 integrity. PLoS Pathog 6:e1000957.
623 36. Ates LS, van der Woude AD, Bestebroer J, van Stempvoort G, Musters RJ, Garcia-Vallejo JJ,
624 Picavet DI, Weerd R, Maletta M, Kuijl CP, van der Wel NN, Bitter W. 2016. The ESX-5 System
625 of Pathogenic Mycobacteria Is Involved In Capsule Integrity and Virulence through Its
626 Substrate PPE10. PLoS Pathog 12:e1005696.
627 37. Nath Y, Ray SK, Buragohain AK. 2018. Essential role of the ESX-3 associated eccD3 locus in
628 maintaining the cell wall integrity of Mycobacterium smegmatis. Int J Med Microbiol
629 308:784-795.
630 38. Bosserman RE, Champion PA. 2017. Esx Systems and the Mycobacterial Cell Envelope:
631 What's the Connection? J Bacteriol 199.
632 39. Bottai D, Di Luca M, Majlessi L, Frigui W, Simeone R, Sayes F, Bitter W, Brennan MJ, Leclerc
633 C, Batoni G, Campa M, Brosch R, Esin S. 2012. Disruption of the ESX-5 system of
634 Mycobacterium tuberculosis causes loss of PPE protein secretion, reduction of cell wall
635 integrity and strong attenuation. Mol Microbiol 83:1195-209.
636 40. Thomas KJ, 3rd, Rice CV. 2014. Revised model of calcium and magnesium binding to the
637 bacterial cell wall. Biometals 27:1361-70.
638 41. Pedersen UR, Leidy C, Westh P, Peters GH. 2006. The effect of calcium on the properties of
639 charged phospholipid bilayers. Biochim Biophys Acta 1758:573-82.

640 42. Melcrova A, Pokorna S, Pullanchery S, Kohagen M, Jurkiewicz P, Hof M, Jungwirth P, Cremer
641 PS, Cwiklik L. 2016. The complex nature of calcium cation interactions with phospholipid
642 bilayers. Sci Rep 6:38035.
643 43. Ginez LD, Osorio A, Vazquez-Ramirez R, Arenas T, Mendoza L, Camarena L, Poggio S. 2022.
644 Changes in fluidity of the E. coli outer membrane in response to temperature, divalent
645 cations and polymyxin-B show two different mechanisms of membrane fluidity adaptation.
646 FEBS J 289:3550-3567.
647 44. Schindler M, Osborn MJ. 1979. Interaction of divalent cations and polymyxin B with
648 lipopolysaccharide. Biochemistry 18:4425-30.
649 45. Xie Y, Yang L. 2016. Calcium and Magnesium Ions Are Membrane-Active against Stationary-
650 Phase Staphylococcus aureus with High Specificity. Sci Rep 6:20628.
651 46. Asif A, Mohsin H, Tanvir R, Rehman Y. 2017. Revisiting the Mechanisms Involved in Calcium
652 Chloride Induced Bacterial Transformation. Front Microbiol 8:2169.
653 47. Fujimoto DF, Bayles KW. 1998. Opposing roles of the Staphylococcus aureus virulence
654 regulators, Agr and Sar, in Triton X-100- and penicillin-induced autolysis. J Bacteriol
655 180:3724-6.
656 48. Cheung GY, Wang R, Khan BA, Sturdevant DE, Otto M. 2011. Role of the accessory gene
657 regulator agr in community-associated methicillin-resistant Staphylococcus aureus
658 pathogenesis. Infect Immun 79:1927-35.
659 49. Zielinska AK, Beenken KE, Joo HS, Mrak LN, Griffin LM, Luong TT, Lee CY, Otto M, Shaw LN,
660 Smeltzer MS. 2011. Defining the strain-dependent impact of the Staphylococcal accessory
661 regulator (sarA) on the alpha-toxin phenotype of Staphylococcus aureus. J Bacteriol
662 193:2948-58.
663 50. Grein F, Muller A, Scherer KM, Liu X, Ludwig KC, Klockner A, Strach M, Sahl HG, Kubitscheck
664 U, Schneider T. 2020. Ca(2+)-Daptomycin targets cell wall biosynthesis by forming a
665 tripartite complex with undecaprenyl-coupled intermediates and membrane lipids. Nat
666 Commun 11:1455.
667 51. Muller A, Wenzel M, Strahl H, Grein F, Saaki TNV, Kohl B, Siersma T, Bandow JE, Sahl HG,
668 Schneider T, Hamoen LW. 2016. Daptomycin inhibits cell envelope synthesis by interfering
669 with fluid membrane microdomains. Proc Natl Acad Sci U S A 113:E7077-E7086.
670 52. Jones T, Yeaman MR, Sakoulas G, Yang SJ, Proctor RA, Sahl HG, Schrenzel J, Xiong YQ, Bayer
671 AS. 2008. Failures in clinical treatment of Staphylococcus aureus Infection with daptomycin
672 are associated with alterations in surface charge, membrane phospholipid asymmetry, and
673 drug binding. Antimicrob Agents Chemother 52:269-78.
674 53. Mishra NN, Bayer AS. 2013. Correlation of cell membrane lipid profiles with daptomycin
675 resistance in methicillin-resistant Staphylococcus aureus. Antimicrob Agents Chemother
676 57:1082-5.
677 54. Ernst CM, Peschel A. 2019. MprF-mediated daptomycin resistance. Int J Med Microbiol
678 309:359-363.
679 55. Mehta S, Cuirolo AX, Plata KB, Riosa S, Silverman JA, Rubio A, Rosato RR, Rosato AE. 2012.
680 VraSR two-component regulatory system contributes to mprF-mediated decreased
681 susceptibility to daptomycin in in vivo-selected clinical strains of methicillin-resistant
682 Staphylococcus aureus. Antimicrob Agents Chemother 56:92-102.

683 56. Nguyen AH, Hood KS, Mileykovskaya E, Miller WR, Tran TT. 2022. Bacterial cell membranes
684 and their role in daptomycin resistance: A review. Front Mol Biosci 9:1035574.
685 57. Rostovtseva TK, Aguilella VM, Vodyanoy I, Bezrukov SM, Parsegian VA. 1998. Membrane
686 surface-charge titration probed by gramicidin A channel conductance. Biophys J 75:1783-
687 92.
688 58. Bobrovskyy M, Chen X, Missiakas D. 2023. The Type 7b Secretion System of S. aureus and
689 Its Role in Colonization and Systemic Infection. Infect Immun 91:e0001523.
690 59. Shariati A, Dadashi M, Moghadam MT, van Belkum A, Yaslianifard S, Darban-Sarokhalil D.
691 2020. Global prevalence and distribution of vancomycin resistant, vancomycin
692 intermediate and heterogeneously vancomycin intermediate Staphylococcus aureus
693 clinical isolates: a systematic review and meta-analysis. Sci Rep 10:12689.
694 60. Machado H, Weng LL, Dillon N, Seif Y, Holland M, Pekar JE, Monk JM, Nizet V, Palsson BO,
695 Feist AM. 2019. Strain-Specific Metabolic Requirements Revealed by a Defined Minimal
696 Medium for Systems Analyses of Staphylococcus aureus. Appl Environ Microbiol 85.
697 61. Wenzel M, Vischer NOE, Strahl H, Hamoen LW. 2018. Assessing Membrane Fluidity and
698 Visualizing Fluid Membrane Domains in Bacteria Using Fluorescent Membrane Dyes. Bio
699 Protoc 8:e3063.
700

701

702 **Figure Legends**

703 **Figure 1. An *esxC* mutant is highly sensitive to daptomycin.**

704 **A)** Growth curves of *S. aureus* WT USA300 JE2 and Δ*esxC* in TSB in the absence or presence
705 of 5 µg/ml daptomycin and 1 mM $CaCl_2$. Mean ± standard error of the mean (SEM) is shown, N =
706 3 (biological replicates). **B)** CFU/ml was enumerated after 8 h daptomycin treatment. N = 3
707 (biological replicates), mean + standard deviation (SD), *** P ≤ 0.001 using an unpaired t-test **C)**
708 Growth curves of USA300 JE2 WTpOS1, Δ*esxC*pOS1 and complemented strain, Δ*esxC*pOS1-
709 *esxC* in TSB supplemented with 5 µg/ml daptomycin and 1 mM $CaCl_2$. Mean ± SEM shown, N =
710 3 (biological replicates); AUC was calculated for the strains grown in presence of daptomycin **(D)**
711 Mean + SD ** P ≤ 0.05 using a one-way ANOVA with Tukey's multiple comparison test. **E)** CFU/ml
712 of WT USA300 JE2 and Δ*esxC* were determined from a killing assay in the presence of 10 µg/ml
713 daptomycin and 1 mM $CaCl_2$ at different timepoints. **F)** CFU/ml from killing assay using WT
714 USA300 JE2, Δ*esxC* and Δ*esxC* complemented strains in the absence or presence of 10 µg/ml

715 daptomycin and 1 mM $CaCl_2$ at different timepoints, mean ± SD, N = 3 (biological replicates), * P
716 ≤ 0.05, ** P ≤ 0.01, *** P ≤ 0.001 using a two-way ANOVA with Tukey multiple comparison test.
717
718 **Figure 2. Membrane permeability of the *esxC* mutant in the presence of daptomycin**
719 **A)** Representative fluorescent micrographs of *S. aureus* USA300 JE2 WT and Δ*esxC* treated with
720 daptomycin. Cell membranes were stained by FM1-43 and imaged using FITC filter channel, PI
721 was imaged using Texas red filter channel. **B)** Images of daptomycin-treated samples (A) were
722 quantified using FIJI. Mean fluorescence intensity was quantified from 10 images from each
723 experiment and normalised to the number of cells in the field of view. Data presented is from 3
724 independent experiments. ****P < 0.0001 using an unpaired t test.
725
726 **Figure 3. The *esxC* mutant show higher sensitivity to other membrane acting drugs**
727 **A)** Growth curves of USA300 JE2 WT and Δ*esxC* in the presence of 2 µg/ml gramicidin, Mean ±
728 SEM, N = 3 (biological replicates). **B)** Area under curves (AUC) were calculated and the mean
729 AUC + SD was plotted for growth curves in (A). **C)** Growth curves of USA300 JE2 WT and Δ*esxC*
730 in the presence of 1 µg/ml bithionol. Mean ± SEM, N = 3 (biological replicates). **D)** AUC were
731 calculated and the mean AUC + SD was plotted for growth curves in (C). *P ≤ 0.05 using an
732 unpaired t-test.
733
734 **Figure 4. EsxC affects membrane fluidity.**
735 **A)** Widefield micrographs of *S. aureus* WT USA300 JE2 and Δ*esxC* after growth in TSB to OD_{600}
736 of 1.0 in the presence of the lipophilic dye DiIC12. Images are representative of 4 independent
737 experiments. The DiIC12 fluorescence of 80 bacterial clusters from different fields per strain was
738 quantitated with ImageJ. Means + SD are shown, N = 4 (biological replicates); **** P < 0.0001,
739 using an unpaired t-test. **B)** The membrane fluidity of *S. aureus* WT USA300 JE2, Δ*esxC* and
740 Δ*esxC* pOS1-*esxC* as measured with a pyrene decanoic acid staining-based assay. Mean ± SEM

741 are shown, N = 6 (biological replicates), * indicates P < 0.05 using a one-way ANOVA. **C)** USA300
742 JE2 WT, Δ*esxC* and Δ*esxC* pOS1-*esxC* were grown to logarithmic phase in TSB at 37ºC prior to
743 staining with Laurdan. To assess membrane fluidity, Laurdan generalised polarisation (GP) was
744 calculated using the equation $(I_{460} – I_{500})/ (I_{460} + I_{500})$ where I refers to the fluorescence intensity at
745 the indicated emission wavelength. *** P <0.0001 using a one-way ANOVA, N = 3 (biological
746 replicates), mean + SD.
747
748 **Figure 5. The *esxC* mutant displays distinct surface morphologies.**
749 **A)** Representative SEM images of *S. aureus* WT USA300 JE2 and *ΔesxC* grown to early
750 logarithmic phase. **B)** Representative SEM images of *S. aureus* USA300 JE2 WT pOS1, *ΔesxC*
751 pOS1, *ΔesxC* pOS1-*esxC* grown to early logarithmic phase.
752
753 **Figure 6. EsxC impacts cell wall synthesis.**
754 **A)** Representative widefield micrographs of *S. aureus* WT USA300 JE2 and *ΔesxC* either grown
755 to logarithmic phase in the presence of 25 μM HADA or after 10-minute treatment with HADA once
756 OD_{600} of 1 was reached. **B)** Quantification of fluorescence in cells grown to logarithmic phase with
757 HADA. **C)** Quantification of fluorescence in cells treated with HADA for 10 minutes. Quantification
758 performed on five images each from 3 independent experiments. * P< 0.01, and using an unpaired
759 t test.
760
761 **Figure 7. EsxC mutant binds more to daptomycin.**
762 **A-B)** Quantitative binding assay of cytochrome C to USA300 JE2 WT, Δ*esxC* and Δ*esxC* pOS1-
763 *esxC* (A). The CFU of the starting inoculum was enumerated for each mutant (B). Mean ± SD
764 shown, N = 3 (biological replicates), ***P < 0.001 using a one-way ANOVA. **C)** Fluorescence
765 measurements of daptomycin-BODIPY upon binding to *S. aureus* WT USA300 JE2 and Δ*esxC.*
766 The excitation wavelength was 488 nm and emission wavelength was 530 nm. N = 3 (biological

767 replicates), mean + SD. P = 0.0067, using an unpaired t-test. **D)** Representative micrographs of
768 daptomycin-BODIPY binding to *S. aureus* WT and Δ*esxC* are shown.
769
770 **Figure 8. Calcium affects growth of *esxC* mutant and daptomycin sensitivity**
771 Growth curves of *S. aureus* WT USA300 JE2, Δ*esxC*, and Δ*esxC* pOS1-*esxC* in synthetic minimal
772 medium in the absence (A) or presence (B) of 50 mM $CaCl_2$. Mean ± standard error of the mean
773 (SEM) is shown **C)** Area under curves (AUC) were calculated from (A) and (B) and the mean AUC
774 ± SD were plotted. **D)** *S. aureus* WT USA300 JE2, Δ*esxC*, and Δ*esxC* pOS1-*esxC* were grown in
775 TSB supplemented with increasing calcium chloride concentrations (0 to 20 mM) in the presence
776 of daptomycin (5 µg/ml). AUCs calculated from growth curves shown in Figure S6 are shown.
777 Mean + SD, ***P= 0.0001, ****P <0.0001, using two-way ANOVA.
778
779 **Figure 9. Presence of EsxC affects intracellular bacterial killing by daptomycin.**
780 **A)** CFU counts at various timepoints during epithelial cell infection assay with WT USA300 JE2,
781 and Δ*esxC*. 0 h represents the initial inoculum, 1 h represents the CFU counts that have infected
782 the A549 cells and 4 h and 24 h represent the survival of *S. aureus* in the presence of 20 µg/ml
783 daptomycin, N = 3 (biological replicates), **P<0.05, two-way ANOVA. **B)** Representative confocal
784 micrographs of cells after 1 h infection or 24 h post-infection. DAPI (blue), F-actin (red), and *S.*
785 *aureus* (green, white arrows). **C)** Confocal image quantification from five images each from 3
786 independent experiments after 24 h. Mean ± SD of intensity, is shown, ***P<0.001 using an
787 unpaired t-test.
788
789 **Figure 10. Effect of daptomycin on *esxC* mutants *in vivo.***
790 Mice were infected in the skin with WT USA300 and Δ*esxC* mutant followed by treatment with 10
791 mg/kg daptomycin. **A)** CFU/g skin tissue was counted 24 h post infection (n = 8, 2 lesions/animal).

792 Graphs show mean ± SD, P = 0.0007 using one-way ANOVA. **B)** CFU/g was calculated 72 h post

793 infection (n = 5, 2 lesions/animal), mean ± SD shown, P = 0.0020 using a one-way ANOVA.

794

795 **Table 1.** Proteins significantly changed in Δ*esxC* mutant membrane preparations relative to WT

796 USA300 JE2.

Uniprot ID	**log_2 fold change**	**Adjusted *P* value**	**Description**
A0A0H2XJR2	-5.46	6.21E-08	Pyridine nucleotide-disulfide oxidoreductase
A0A0H2XJ15	-5.34	3.80E-09	TPR domain protein
A0A0H2XIV9	-5.33	1.49E-07	T7SS protein, EssD
A0A0H2XJ90	-4.82	6.92E-09	D-isomer specific 2-hydroxyacid dehydrogenase family protein
A0A0H2XF36	3.62	2.14E-08	Uncharacterised protein
A0A0H2XJV3	3.67	2.26E-08	ABC transporter, ATP-binding protein
A0A0H2XGS2	3.70	1.71E-08	Putative sensor histidine kinase
A0A0H2XG87	4.01	1.59E-08	Bifunctional ligase/repressor BirA
A0A0H2XH85	4.14	1.04E-08	Cobalamin synthesis protein/P47K family protein
A0A0H2XER9	4.38	9.36E-09	LysR family regulatory protein
A0A0H2XEB7	5.25	2.39E-07	Integral membrane protein
A0A0H2XJ96	5.27	1.04E-08	NADH-dependent flavin oxidoreductase
A0A0H2XHU5	5.97	2.55E-09	Putative membrane protein

797

798

799

800 **Table 2. Strains and Plasmids used in this study**

Strain or Plasmid	Description	Source or Reference
Staphylococcus aureus		
USA300 LAC JE2	Plasmid-cured USA300 LAC	BEI Resources (NARSA)
USA300 JE2 *ΔessC*	USA300 LAC JE2 defective for EssC	(Kengmo Tchoupa *et al.,* 2020)
USA300 JE2 *ΔesxC*	USA300 LAC JE2 defective for EsxC	(Kengmo Tchoupa *et al.,* 2020)
USA300 LAC	Community acquired MRSA	(Bae and Schneewind, 2006)
USA300 LAC *ΔesxA*	USA300 LAC defective for EsxA	(Korea *et al.,* 2014)
USA300 LAC Δ*esxB*	USA300 LAC defective for EsxB	(Korea *et al.,* 2014)
Newman	Methicillin-sensitive *S. aureus*	(Bae and Schneewind, 2006)
Newman *ΔesxA*	Newman defective for EsxA	(Korea *et al.,* 2014)
Newman Δ*esxB*	Newman defective for EsxB	(Korea *et al.,* 2014)
RN6390	NCTC8325 derivative, *ΔrbsU, ΔtcaR,* cured of φ11, φ12, and φ13	Tracy Palmer (Kneuper *et al.,* 2014)
RN6390 *ΔessC*	RN6390 defective for EssC	Tracy Palmer (Kneuper *et al.,* 2014)
RN6390 *ΔesxC*	RN6390 defective for EsxC	Tracy Palmer (Kneuper *et al.,* 2014)
Plasmids		
pOS1	Empty vector for complementation	Olaf Schneewind
pOS1-*esxC*	*esxC* complementation vector	(Kengmo Tchoupa *et al.,* 2020)

801

802

803

804 **Supplementary Figure legends and tables**

805 **Figure S1.** Growth curves in TSB for A) *S. aureus* USA300 LAC Δ*esxA* and Δ*esxB*, C) *S. aureus*
806 Newman Δ*esxA* and *ΔesxB*, E) *S. aureus* USA300 JE2 WT and Δ*esxD,* G) *S. aureus* USA300
807 JE2 WT and Δ*essC* I) *S. aureus* RN6390 WT, *ΔessC* and Δ*esxC*, in the absence or presence of
808 5 µg/ml daptomycin and 1 mM $CaCl_2$. Mean ± SEM are shown, N = 3. The AUC was calculated
809 for the growth curves of all strains cultured in presence of daptomycin in A, C, E and G and I are
810 presented as % relative to WT, mean + SD is shown (B, D, F, H, J). * P ≤ 0.05, ** P ≤ 0.01 using
811 a one-sample t test. J) shows AUC of I) ****P ≤ 0.0001, unpaired t test

812

813 **Figure S2**. Growth curves of USA300 JE2 WT, *ΔessC* and Δ*esxC* in the presence of (A) 4 µg/ml
814 ciprofloxacin (B) 0.5 µg/ml mitomycin C. (C) 1 µg/ml oxacillin. (D) 8 µg/ml vancomycin. For all
815 growth curves mean and SEM are shown, N = 3 (biological replicates).

816

817 **Figure S3.** Scanning electron micrographs of *S. aureus* RN6390, USA300, Newman and their
818 T7SS mutants.

819

820 **Figure S4.** Transmission electron micrographs of *S. aureus* USA300 JE2 WT and Δ*esxC* grown
821 to early logarithmic phase.

822

823 **Figure S5.** Quantitative binding assay of cytochrome C to USA300 LAC WT, Δ*esxA* and Δ*esxB*
824 **(A**). The CFU of the starting inoculum was calculated for each mutant **(B)**. Mean ± SD shown, N
825 = 3 (biological replicates), ***P < 0.001 using a one-way ANOVA

826

827 **Figure S6.** Growth curves of WT, *ΔesxC*, Δ*esxC* pOS1-*esxC* in TSB supplemented with
828 increasing calcium chloride concentrations (0 to 20 mM) in the presence of 5 µg/ml daptomycin.
829 Mean +SE is shown

830

831 **Figure S7. (A)** Growth curves of WT, Δ*essC* and Δ*esxC* in DMEM + FBS. **(B)** Growth curves of
832 WT, Δ*essC* and Δ*esxC* in DMEM + FBS in the presence of 1 µg/ml daptomycin and 1 mM $CaCl_2$.
833 Graphs show mean and SEM of three independent experiments.

834

835 **Figure S8** The area of lesions was measured and calculated daily from mice infected with *S.*
836 *aureus* WT or T7SS mutant.. Graph shows mean ± SD. Two-way ANOVA between groups
837 revealed no significant differences between treatments.

838 **Table S**1 Secreted proteins significantly changed in Δ*esxC* and Δ*essC* mutants relative to WT
839 USA300 JE2.

840

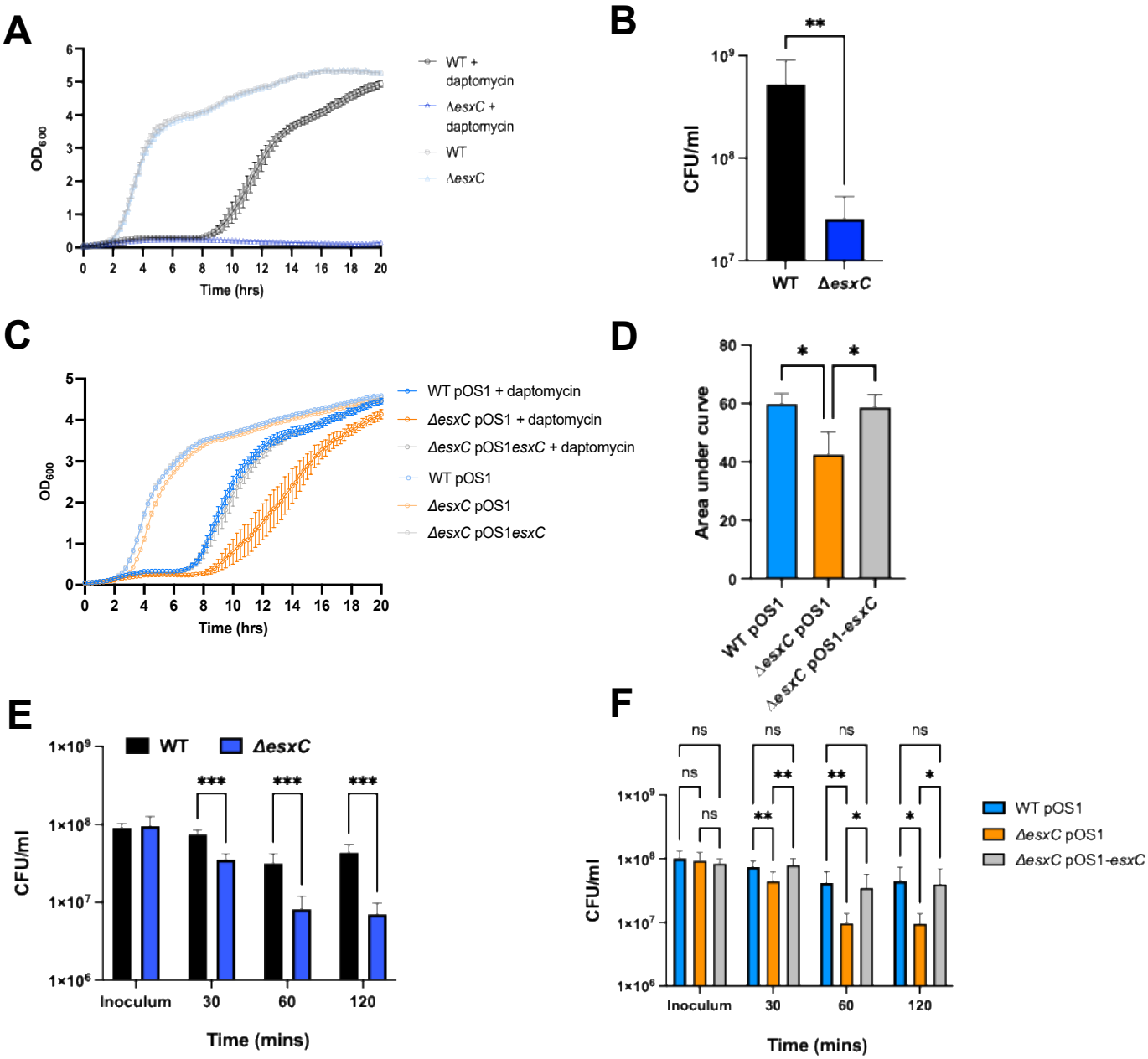

Figure 1. An *esxC* mutant is highly sensitive to daptomycin.
A) Growth curves of *S. aureus* WT USA300 JE2 and Δ*esxC* in TSB in the absence or presence of 5 µg/ml daptomycin and 1 mM $CaCl_2$. Mean ± standard error of the mean (SEM) is shown, N = 3 (biological replicates). **B)** CFU/ml was enumerated after 8 h daptomycin treatment. N = 3 (biological replicates), mean + standard deviation (SD), *** P ≤ 0.001 using an unpaired t-test **C)** Growth curves of USA300 JE2 WTpOS1, Δ*esxC*pOS1 and complemented strain, Δ*esxC*pOS1-*esxC* in TSB supplemented with 5 µg/ml daptomycin and 1 mM $CaCl_2$. Mean ± SEM shown, N = 3 (biological replicates); AUC was calculated for the strains grown in presence of daptomycin **(D)** Mean + SD ** P ≤ 0.05 using a one-way ANOVA with Tukey's multiple comparison test. **E)** CFU/ml of WT USA300 JE2 and Δ*esxC* were determined from a killing assay in the presence of 10 µg/ml daptomycin and 1 mM $CaCl_2$ at different timepoints. **F)** CFU/ml from killing assay using WT USA300 JE2, Δ*esxC* and Δ*esxC* complemented strains in the absence or presence of 10 µg/ml daptomycin and 1 mM $CaCl_2$ at different timepoints, mean ± SD, N = 3 (biological replicates), * P ≤ 0.05, ** P ≤ 0.01, *** P ≤ 0.001 using a two-way ANOVA with Tukey multiple comparison test.

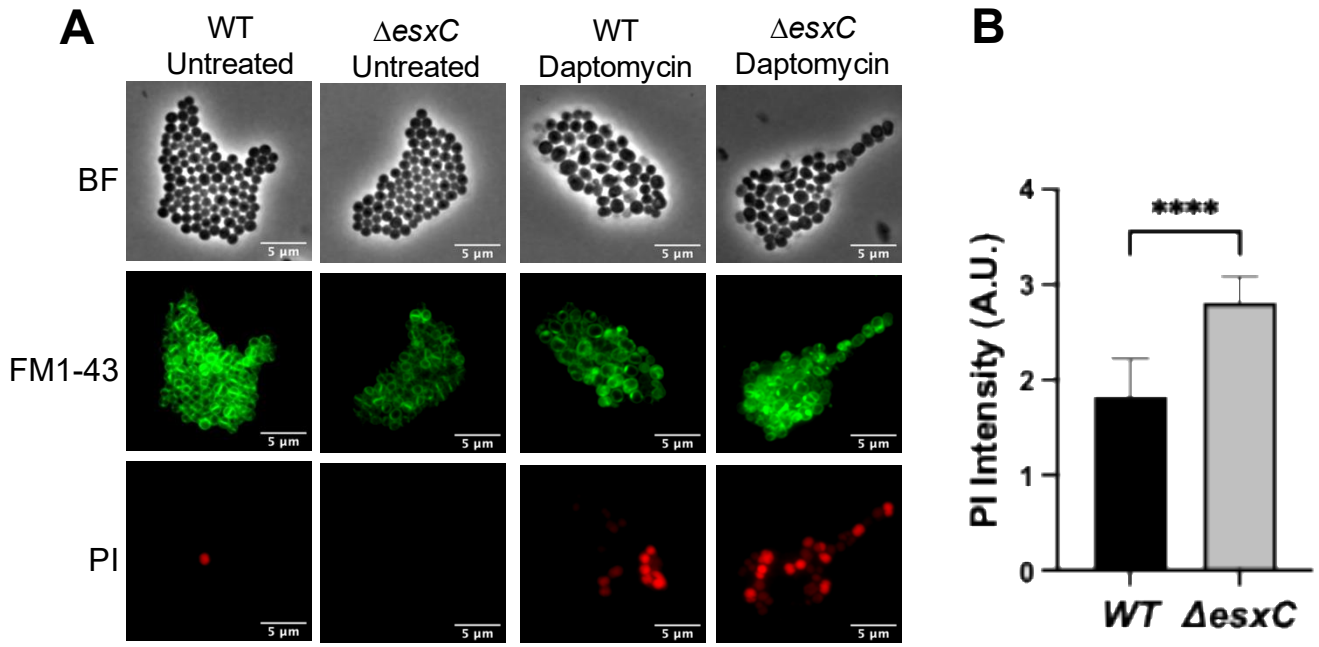

Figure 2. Membrane permeability of the *esxC* mutant in the presence of daptomycin

A) Representative fluorescent micrographs of *S. aureus* USA300 JE2 WT and Δ*esxC* treated with daptomycin. Cell membranes were stained by FM1-43 and imaged using FITC filter channel, PI was imaged using Texas red filter channel. **B)** Images of daptomycin-treated samples (A) were quantified using FIJI. Mean fluorescence intensity was quantified from 10 images from each experiment and normalised to the number of cells in the field of view. Data presented is from 3 independent experiments. ****$P < 0.0001$ using an unpaired t test.

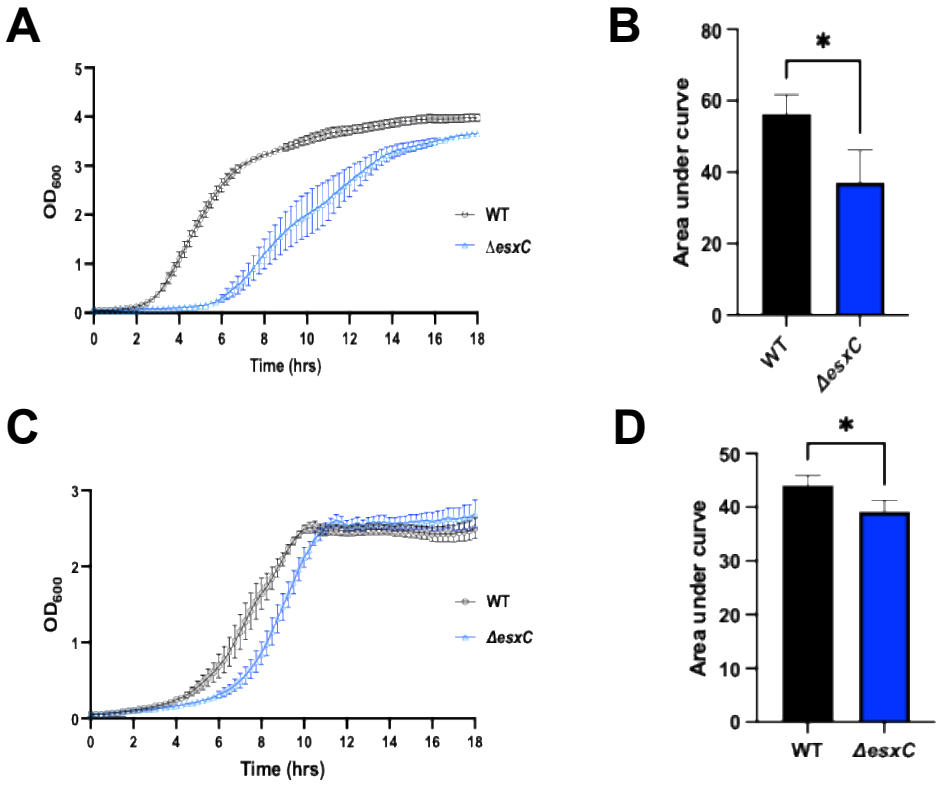

Figure 3. The *esxC* mutant show higher sensitivity to other membrane acting drugs

A) Growth curves of USA300 JE2 WT and Δ*esxC* in the presence of 2 µg/ml gramicidin, Mean ± SEM, N = 3 (biological replicates). **B)** Area under curves (AUC) were calculated and the mean AUC + SD was plotted for growth curves in (A). **C)** Growth curves of USA300 JE2 WT and Δ*esxC* in the presence of 1 µg/ml bithionol. Mean ± SEM, N = 3 (biological replicates). **D)** AUC were calculated and the mean AUC + SD was plotted for growth curves in (C). *P ≤ 0.05 using an unpaired t-test.

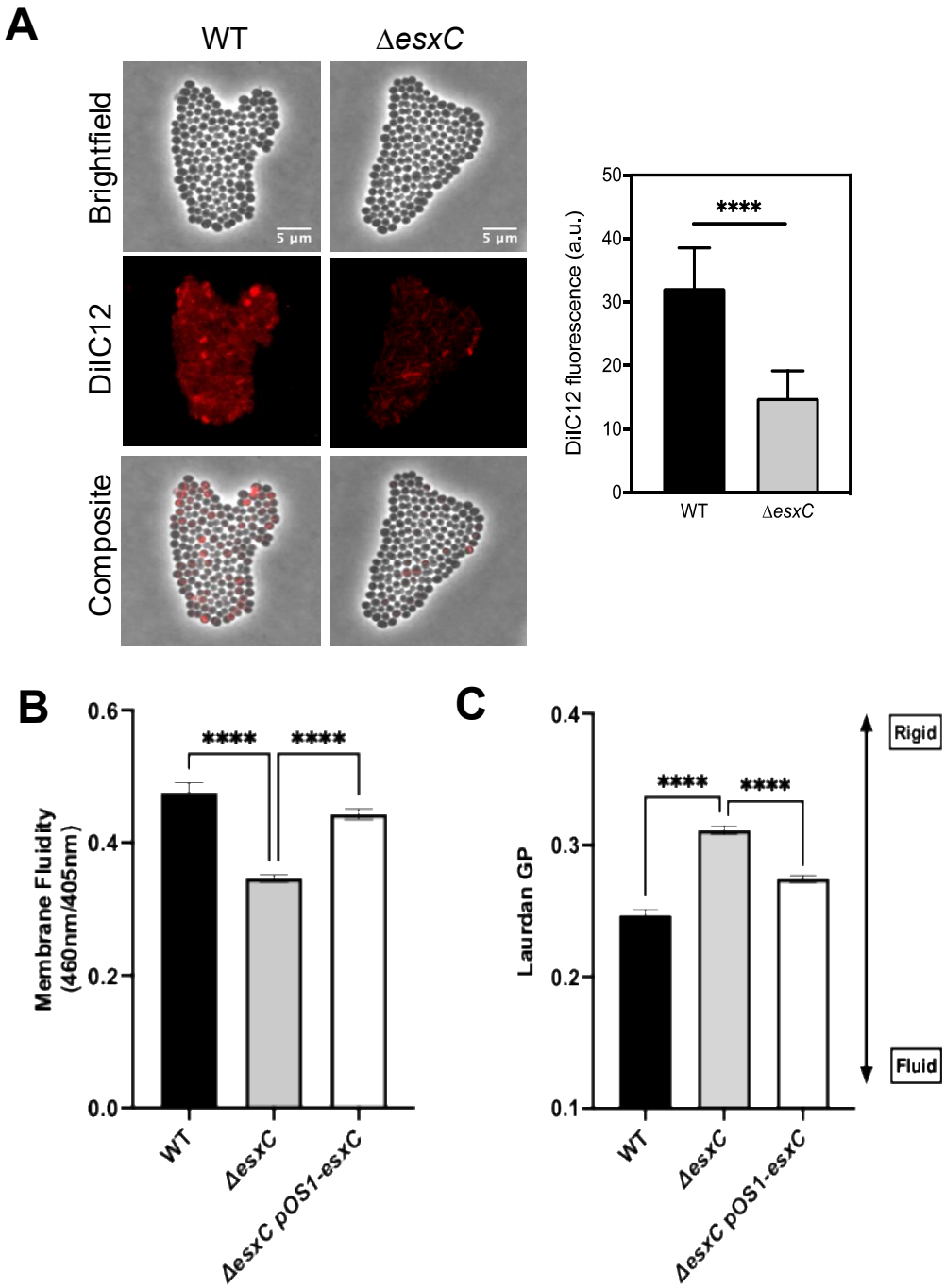

Figure 4. EsxC affects membrane fluidity

A) Widefield micrographs of *S. aureus* WT USA300 JE2 and Δ*esxC* after growth in TSB to OD_{600} of 1.0 in the presence of the lipophilic dye DiIC12. Images are representative of 4 independent experiments. The DiIC12 fluorescence of 80 bacterial clusters from different fields per strain was quantitated with ImageJ. Means + SD are shown, N = 4 (biological replicates); **** P < 0.0001, using an unpaired t-test. **B)** The membrane fluidity of *S. aureus* WT USA300 JE2, Δ*esxC* and Δ*esxC* pOS1-*esxC* as measured with a pyrene decanoic acid staining-based assay. Mean ± SEM are shown, N = 6 (biological replicates), * indicates P < 0.05 using a one-way ANOVA. **C)** USA300 JE2 WT, Δ*esxC* and Δ*esxC* pOS1-*esxC* were grown to logarithmic phase in TSB at 37ºC prior to staining with Laurdan. To assess membrane fluidity, Laurdan generalised polarisation (GP) was calculated using the equation $(I_{460} - I_{500})/(I_{460} + I_{500})$ where I refers to the fluorescence intensity at the indicated emission wavelength. *** P <0.0001 using a one-way ANOVA, N = 3 (biological replicates), mean + SD.

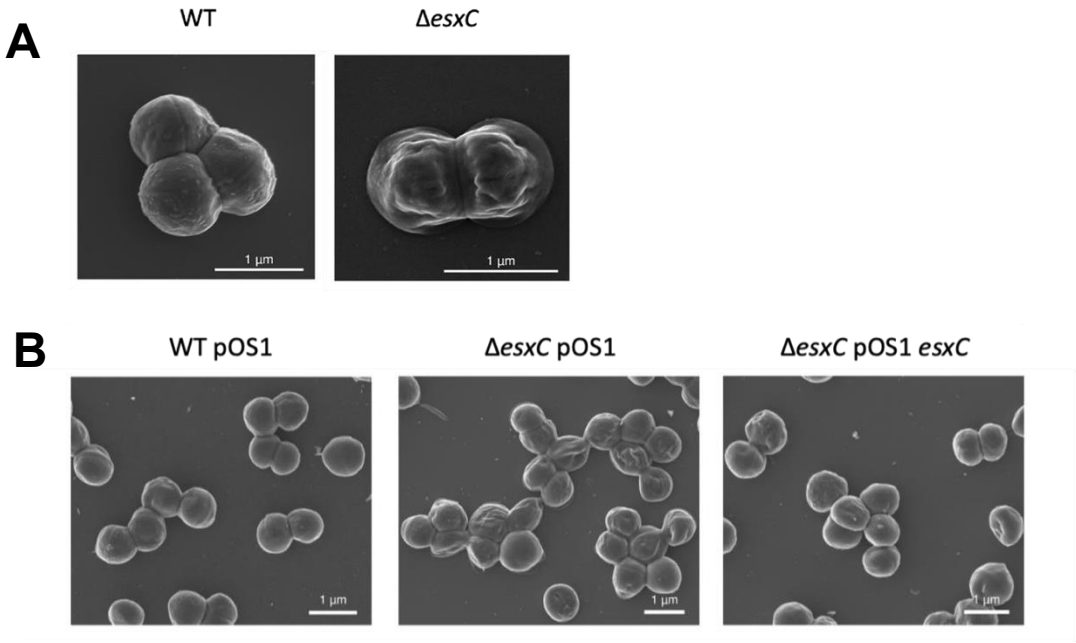

Figure 5. The *esxC* mutant displays distinct surface morphology.

A) Representative SEM images of *S. aureus* WT USA300 JE2 and *ΔesxC* grown to early logarithmic phase. **B)** Representative SEM images of *S. aureus* USA300 JE2 WTpOS1, *ΔesxC*pOS1, *ΔesxC*pOS1-*esxC* grown to early logarithmic phase.

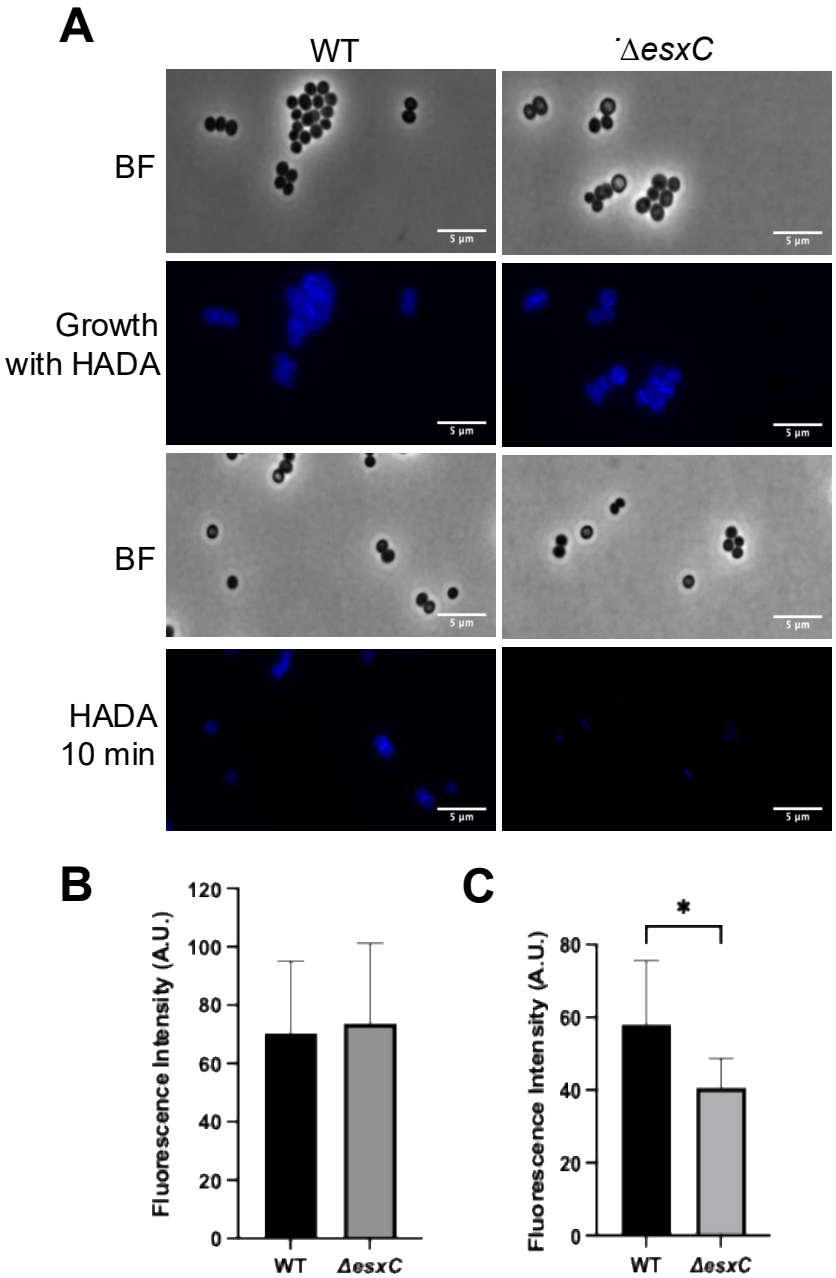

Figure 6. EsxC impacts cell wall synthesis.
A) Representative widefield micrographs of *S. aureus* WT USA300 JE2 and *ΔesxC* either grown to logarithmic phase in the presence of 25 µM HADA or after 10-minute treatment with HADA once OD_{600} of 1 was reached. **B)** Quantification of fluorescence in cells grown to logarithmic phase with HADA. **C)** Quantification of fluorescence in cells treated with HADA for 10 minutes. Quantification performed on five images each from 3 independent experiments. * $P < 0.01$, and by an unpaired t test.

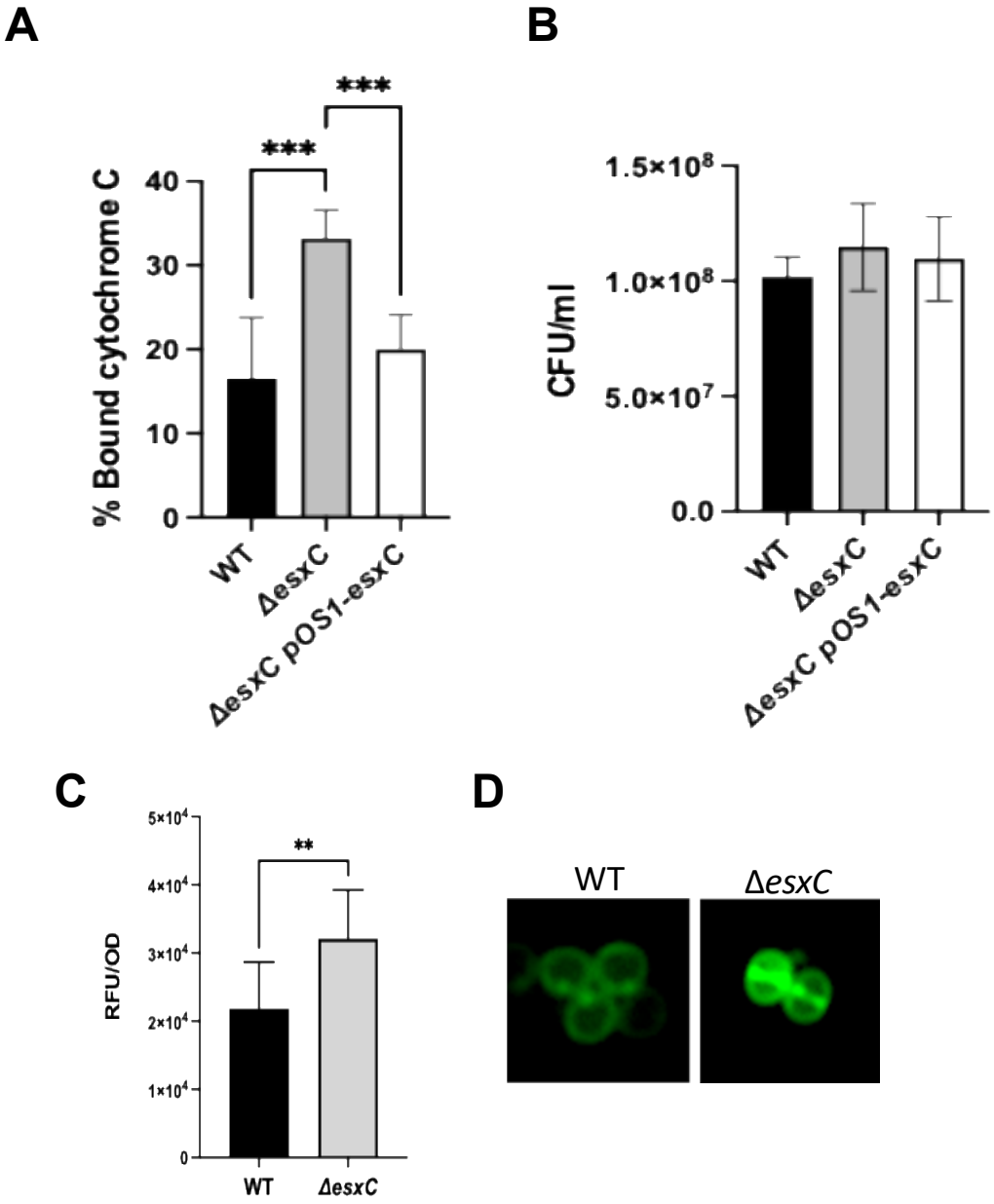

Figure 7. EsxC mutant membranes bind more to daptomycin.
Quantitative binding assay of cytochrome C to USA300 JE2 WT, Δ*esxC* and Δ*esxC*pOS1-*esxC* **(A**). The CFU of the starting inoculum was calculated for each mutant **(B)**. Mean ± SD shown, N = 3 (biological replicates), ***P < 0.001 using a one-way ANOVA. **C)** Fluorescence measurements of daptomycin-BODIPY binding to *S. aureus* WT USA300 JE2 and Δ*esxC.* The excitation wavelength was 488nm and emission wavelength was 530nm. N = 3 (biological replicates), mean ± SD. P = 0.0067, using an unpaired t-test. **D)** Representative micrographs of daptomycin-BODIPY binding to *S. aureus* WT and Δ*esxC* are shown.

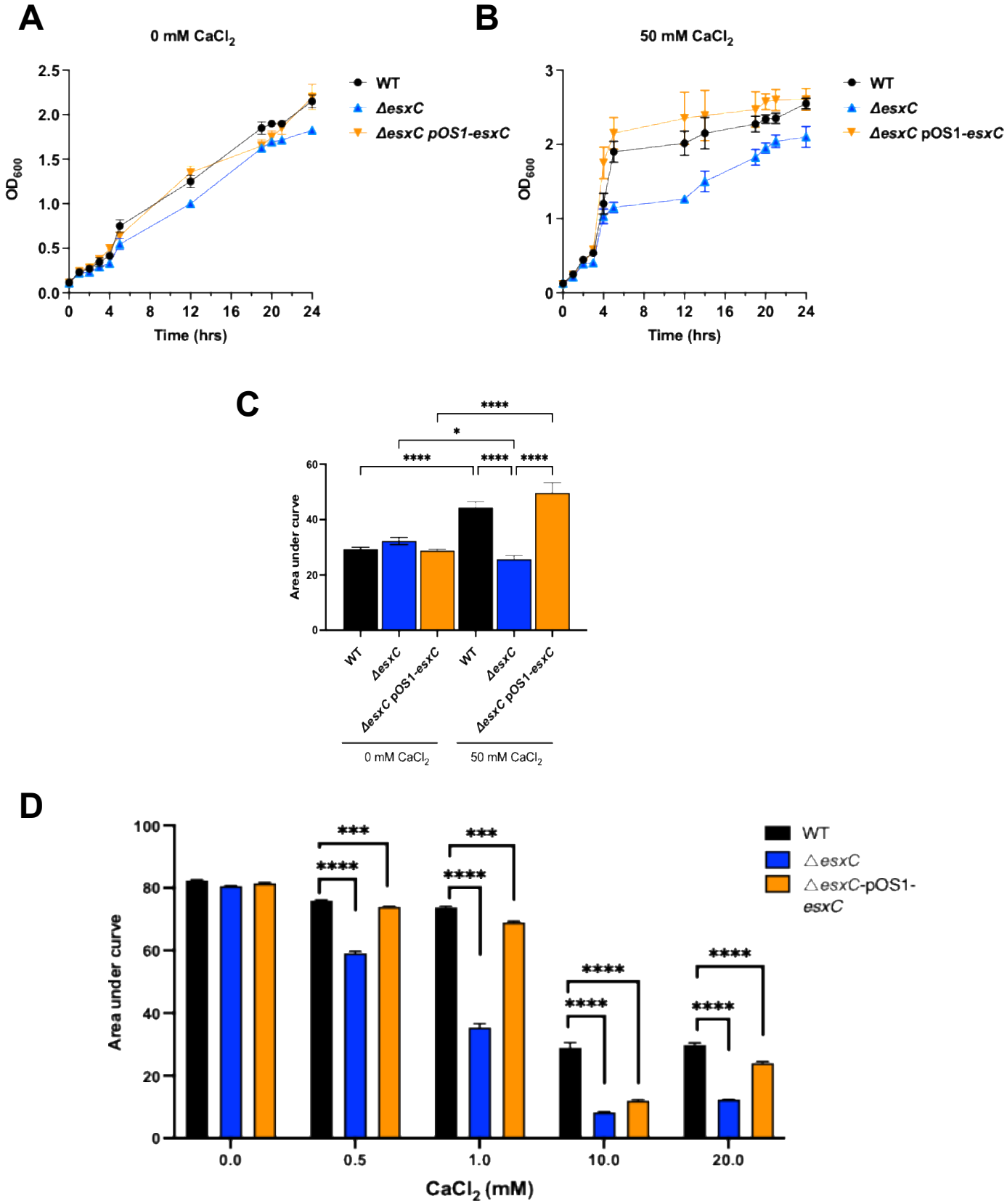

Figure 8. Calcium affects growth of *esxC* mutant and daptomycin sensitivity
Growth curves of *S. aureus* WT USA300 JE2, Δ*esxC*, and Δ*esxC* pOS1-*esxC* in synthetic minimal medium in the absence (A) or presence (B) of 50 mM $CaCl_2$. Mean ± standard error of the mean (SEM) is shown **C)** Area under curves (AUC) were calculated from (A) and (B) and the mean AUC ± SD were plotted. **D)** *S. aureus* WT USA300 JE2, Δ*esxC*, and Δ*esxC* pOS1-*esxC* were grown in TSB supplemented with increasing calcium chloride concentrations (0 to 20 mM) in the presence of daptomycin (5 µg/ml). AUCs calculated from growth curves shown in Figure S6 are shown. Mean + SD, ***P= 0.0001, ****P <0.0001, using two-way ANOVA.

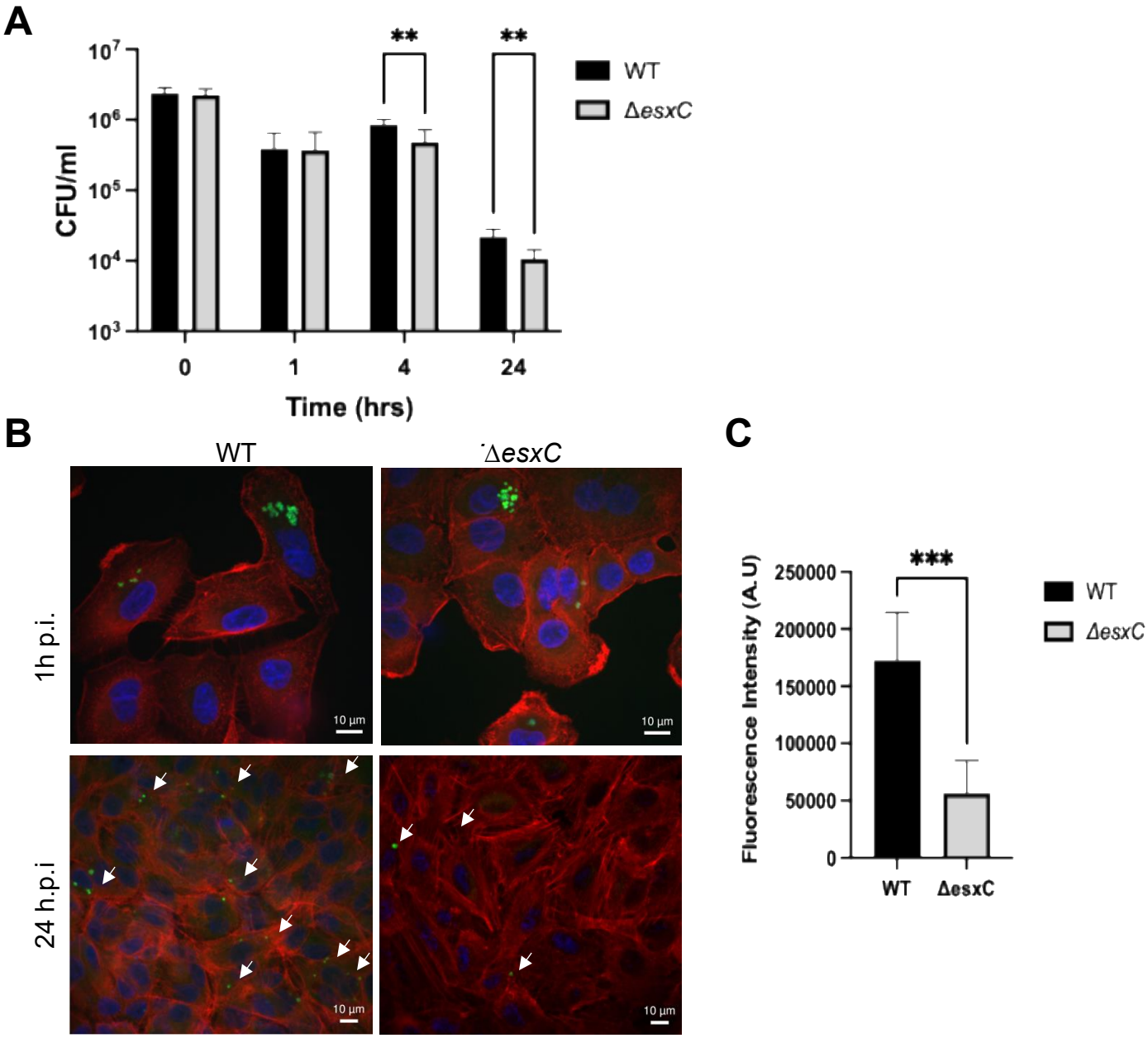

Figure 9. Presence of EsxC affects intracellular bacterial killing by daptomycin.
A) CFU counts at various timepoints during epithelial cell infection assay with WT USA300 JE2, and Δ*esxC*. 0 h represents the initial inoculum, 1 h represents the CFU counts that have infected the A549 cells and 4 h and 24 h represent the survival of *S. aureus* in the presence of 20 µg/ml daptomycin, N = 3 (biological replicates), **P<0.05, two-way ANOVA. **B)** Representative confocal micrographs of cells after 1 h infection or 24 h post-infection. DAPI (blue), F-actin (red), and *S. aureus* (green, white arrows). **C)**Confocal image quantification from five images each from 3 independent experiments after 24 h. Mean ± SD of intensity, is shown, ***P<0.001 using an unpaired t-test.

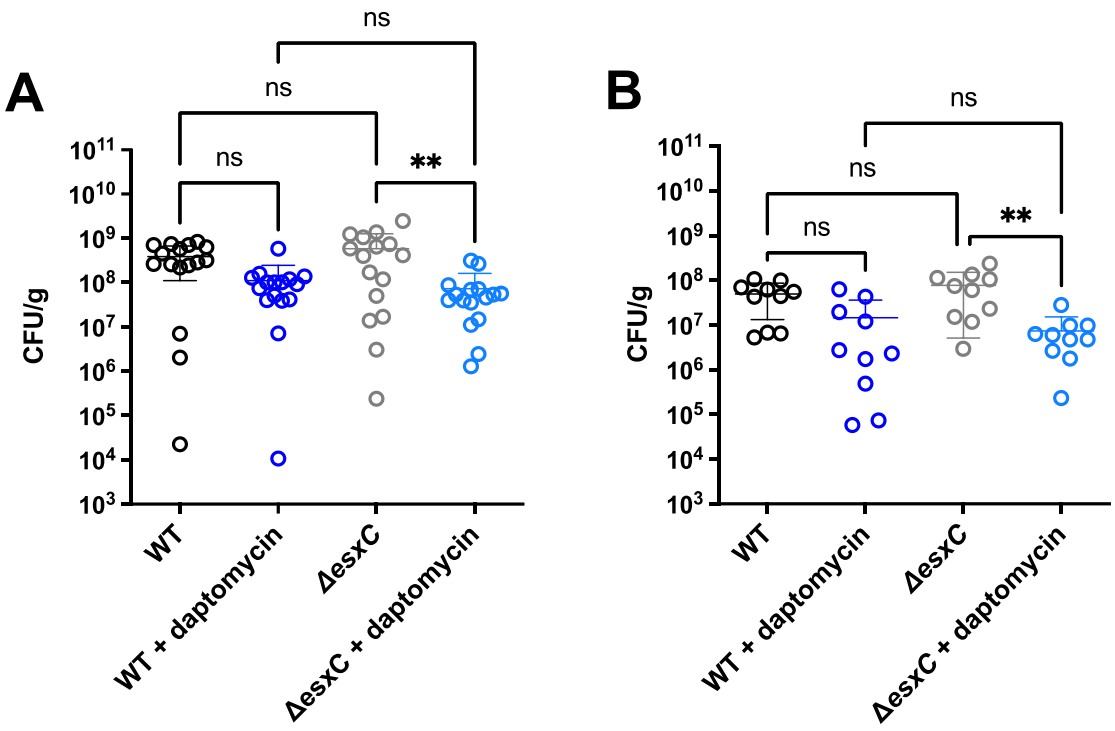

Figure 10. Effect of daptomycin on *esxC* mutants *in vivo.*

Mice were infected in the skin with WT USA300 and Δ*esxC* mutant followed by treatment with 10 mg/kg daptomycin. **A)** CFU/g skin tissue was counted 24 h post infection (n = 8, 2 lesions/animal). Graphs show mean ± SD, P = 0.0007 using one-way ANOVA. **B)** CFU/g was calculated 72 h post infection (n = 5, 2 lesions/animal), mean ± SD shown, P = 0.0020 using a one-way ANOVA.